AD-A066 175 NAVAL RESEARCH LAB WASHINGTON D C F/G 4/1
A REVIEW OF RECENT RESULTS ON SPREAD F THEORY.(U)
JAN 79 S L OSSAKOW
UNCLASSIFIED NRL-MR-3909 SBIE-AD-E000 273 NL

END
DATE FILMED
5-79
DDC

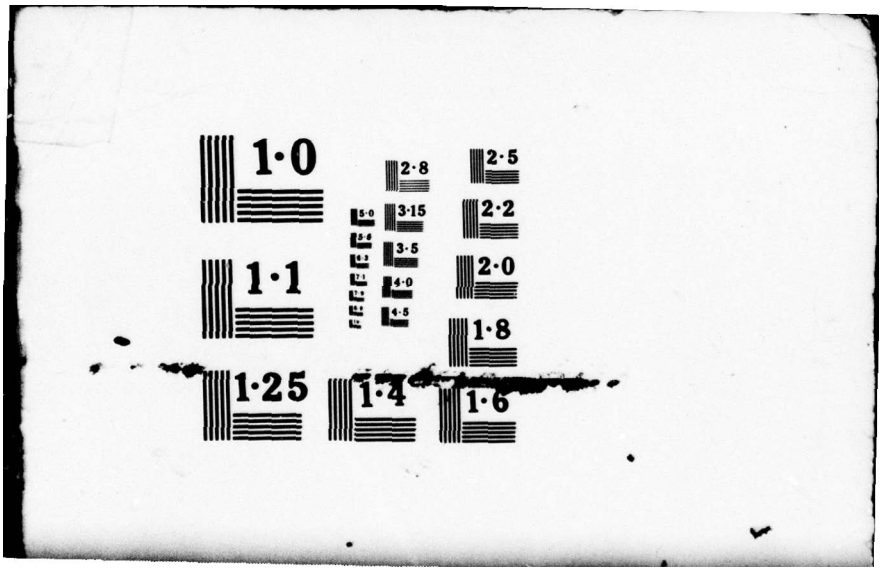
1·0
1·1
1·25
1·4
1·6
1·8
2·0
2·2
2·5
2·8
3·15
3·5
4·0
4·5

(13) NW LEVEL III

SECURITY CLASSIFICATION OF THIS PAGE (When Data Entered)

REPORT DOCUMENTATION PAGE

READ INSTRUCTIONS BEFORE COMPLETING FORM

1. REPORT NUMBER: NRL Memorandum Report 3909 (14) NRL-MR-
2. GOVT ACCESSION NO.
3. RECIPIENT'S CATALOG NUMBER (9)

4. TITLE (and Subtitle): (6) A REVIEW OF RECENT RESULTS ON SPREAD F THEORY
5. TYPE OF REPORT & PERIOD COVERED: Interim report on a continuing NRL problem
6. PERFORMING ORG. REPORT NUMBER

7. AUTHOR(s): (10) S. L. Ossakow
8. CONTRACT OR GRANT NUMBER(s)

9. PERFORMING ORGANIZATION NAME AND ADDRESS: Naval Research Laboratory, Washington, D.C. 20375
10. PROGRAM ELEMENT, PROJECT, TASK AREA & WORK UNIT NUMBERS: NRL Problem H02-42D and A03-16B; (16) DNA Subtask I25AAXYX960

11. CONTROLLING OFFICE NAME AND ADDRESS: Defense Nuclear Agency, Washington, D.C. 20305 and Office of Naval Research, Arlington, Virginia 22217
12. REPORT DATE: January [illegible], 1979 (11) 9 (17)
13. NUMBER OF PAGES: 52 X960

14. MONITORING AGENCY NAME & ADDRESS (if different from Controlling Office): (12) 51p.
15. SECURITY CLASS. (of this report): UNCLASSIFIED
15a. DECLASSIFICATION/DOWNGRADING SCHEDULE

16. DISTRIBUTION STATEMENT (of this Report)

Approved for public release; distribution unlimited.

(18) SBIE

DDC RECEIVED MAR 22 1979 B

17. DISTRIBUTION STATEMENT (of the abstract entered in Block 20, if different from Report)

(19) AD-E000 273

18. SUPPLEMENTARY NOTES

This Research was sponsored partially by the Defense Nuclear Agency under Subtask I25AAXYX960, work unit code 17 and work unit title Scintillation Description, and partially by the Office of Naval Research.

(Continues)

19. KEY WORDS (Continue on reverse side if necessary and identify by block number)

Equatorial Spread F
Theory
Numerical simulations
Review

20. ABSTRACT (Continue on reverse side if necessary and identify by block number)

Although ionospheric Spread F was discovered some four decades ago, yet only in the past few years has significant progress been made in the theoretical explanation of such phenomena. In particular, considerable effort has been expended to explain equatorial Spread F and the attendant satellite signal propagation scintillation phenomena. The present review dwells mainly in this low latitude area. The various linear plasma instabilities thought to initiate equatorial Spread F will be discussed. Recent theoretical and numerical simulation studies of the nonlinear evolution of the collisional

(Continues)

DD FORM 1 JAN 73 1473 EDITION OF 1 NOV 65 IS OBSOLETE
S/N 0102-014-6601

251 950

79 02 08 005

18. Supplementary Notes (Continued)

This paper is based on the presentation made at the XIXth URSI General Assembly, Helsinki, Finland, August 1978.

20. Abstract (Continued)

Rayleigh-Taylor instability in equatorial Spread F ~~will be~~ reviewed. ~~Also,~~ analytical studies of rising equatorial Spread F bubbles in the collisional and collisionless Rayleigh-Taylor regime ~~will be~~ are discussed, as well as the nonlinear saturation of instabilities in these two regimes. Current theories on very small scale ~~(< 10 meters)~~ size irregularities observed by radar backscatter during equatorial Spread F and their relation to the larger wavelength scintillation causing irregularities ~~will be~~ discussed. Application of turbulence theory to equatorial Spread F phenomena ~~will be~~ reviewed. Remaining problems to be dealt with at equatorial latitudes ~~will be~~ summarized.

(approximately < or = 10 meters)

CONTENTS

I. INTRODUCTION 1

II. THEORY 7

III. SUMMARY 25

ACKNOWLEDGMENTS 27

REFERENCES 28

A REVIEW OF RECENT RESULTS ON SPREAD F THEORY

I. Introduction

Spread F, as exhibited by diffuse echoes on ionograms, was discovered some forty years ago by Booker and Wells (1938). Until recently, there has been only much statistical data concerning Spread F. However, in the last few years with advances in radar backscatter measurements, in situ measurements, and theoretical and numerical simulation techniques a clearer picture of the fundamental plasma instability mechanisms causing equatorial Spread F phenomena has been evolving. It should be emphasized that this paper will deal only with equatorial Spread F theory and, in addition, dwell only on those theories using plasma mechanisms as a basis. For experimental results, the works of Farley et al. (1970), Dyson et al. (1974), Kelley et al. (1976), Woodman and La Hoz (1976), Morse et al. (1977), and McClure et al. (1977) should serve as good references for the interested reader.

In speaking about Spread F one should at least show its basic manifestation on an ionogram (see Fig. 1). After all, the terminology Spread F emerged from the results of ionosonde traces such as those exhibited in Fig. 1. The multiple traces are caused by magnetic field aligned irregularities. If there were no irregularities, a single crisp trace rising to the right would be exhibited on the ionogram. At this point we want to remember the basic equatorial geometry. Figure 2 exhibits the basic equatorial nighttime ionospheric F region geometry, i.e., the geometry under which equatorial Spread F occurs.

Note: Manuscript submitted November 16, 1978.

N(y) represents the background electron density as a function of altitude (y). Gravity, $\underline{g}$, points down, the ambient magnetic field, $\underline{B}$, is horizontal (pointing north) and $\underline{k}$ represents a horizontal perturbation (in the westward direction). The maximum in the electron density profile is the F peak. The underside of the profile steepens at night due to chemical recombination effects and electrodynamic forces. The E region has been severely reduced by chemical recombination and plays a negligible role. To a plasma physicist this geometry is a classical flute mode geometry and one might expect this equatorial ionospheric geometry to be unstable to a variety of plasma instabilities. However, until recently, one of the basic difficulties was getting the unstable irregularities to the topside (i.e., above the F peak) when they were initiated on the bottomside. One must remember that the experimental evidence has exhibited both top and bottomside irregularities.

At this point a general brief review will be given of equatorial Spread F (ESF) theories. First, we will discuss the linear theories. Dungey (1956) was the first to suggest that ESF was initiated on the bottomside by a Rayleigh-Taylor instability. Dagg (1957) suggested that the ESF phenomena was due to E to F region coupling, i.e., irregularities in the E region coupled up to the F region. In 1959, Martyn (1959) was the first to suggest that ESF was a manifestation of the $\underline{E} \times \underline{B}$ gradient drift instability. Calvert (1963) proposed that the downward motion of the neutral atmosphere at night was responsible for ESF. This mechanism is essentially equivalent to the $\underline{E} \times \underline{B}$

instability because of the relative motion between ions and neutrals in determining the instability. All of these previously invoked linear instability mechanisms could only explain the formation of bottomside irregularities. The collisional Rayleigh-Taylor instability with field line averaging was also proposed (Balsley et al., 1972; Haerendel, 1974) as a linear instability mechanism. By averaging (integrating) the density along the magnetic field, the total electron content profile becomes steeper on the bottomside and its peak is raised in altitude with respect to the local electron density peak. This would allow the linear mechanism to operate to slightly higher altitudes ($\sim$ 100 km greater), but still would not explain the existence of irregularities above this "new peak". Hudson and Kennel (1975) pointed out the importance of the collisional drift mode in ESF in the wavelength regime 30m - 100m. This mode could be excited on both the top and bottomside but still would not explain the longer wavelengths. In their paper, finite larmor radius (FLR) corrections were also applied to the collisionless and collisional Rayleigh-Taylor instability.

Several nonlinear theories have been invoked to explain the different ESF observations. For example, Hudson et al. (1973) suggested that the very smallest scale ($\lesssim$10m) irregularities (e.g., those seen by radar coherent backscatter) were due to a two step process. In this prescription a longer wavelength instability sets up the driving conditions for the shorter wavelengths to become unstable. This is similar in spirit to the successful two step

theory (Sudan et al., 1973) proposed for Type II equatorial E region electrojet irregularities. Haerendel (1974) suggested that the range of wavelengths (many kilometers down to centimeters) exhibited by ESF phenomena was due to a multi-step process. This scenario is as follows: (i) the collisional Rayleigh-Taylor (R-T) instability with horizontal wavevectors is driven by gravity and the background, zero order electron density gradient scale length on the bottomside; then (ii) the $\underline{E}$ X $\underline{B}$ gradient drift instability with vertical wavevectors arises due to the horizontal density, large amplitude variations set up by the collisional R-T instability; then (iii) the inertia (collisionless) dominated R-T instability arises; and finally (iv) kinetic drift waves grow upon these irregularities after they reach large amplitude. Chaturvedi and Kaw (1976) interpreted the k^{-2} measured power spectrum of the ESF plasma density irregularities in terms of a two step theory. In this theory longer wavelength R-T modes couple to kinetic collisional drift waves in such a manner that the mode coupling results in the observed k^{-2} spectrum.

A major breakthrough was made by Scannapieco and Ossakow (1976) who performed a nonlinear numerical simulation of the collisional R-T instability for ESF geometry. The simulation results showed that the collisional R-T instability generated irregularities and bubbles (plasma density depletions) on the bottomside of the F region which subsequently rose beyond the F peak by nonlinear polarization induced $\underline{E}$ X $\underline{B}$ forces. This was the first theoretical result to explain how long wavelength irregularities could appear on both the bottomside and

topside of the F region. The bubble phenomena was in accord with the recent observations (Kelley et al., 1976; McClure et al., 1977, Woodman and La Hoz, 1976) of plasma density depletions. An analytical nonlinear mode-mode coupling theory for the coherent development of the collisional R-T instability was performed by Chaturvedi and Ossakow (1977). This theory suggested that vertical modes would be dominant and result in a k^{-2} power spectrum. Hudson (1978) extended the previous results to the collisionless R-T regime and reached similar conclusions. Analytical models for the rise of collisional and collisionless R-T ESF bubbles, in analogy with fluid bubbles, was presented by Ott (1978). At the same time, Ossakow and Chaturvedi (1978) presented analytical models for the rise of collisional R-T ESF bubbles within the context of the electrical analogy with barium clouds.

Costa and Kelley (1978a,b) suggested that coherent steepened structures and not turbulences would give a k^{-2} power spectrum. Moreover, these sharp gradients could cause small scale sizes ($\sim$ 20m) by collisionless low frequency (much less than the ion gyrofrequency, Ω_i) kinetic drift waves via a two step process. Their analysis was a linear one carried out on a nonlinear state, i.e., one achieves the steepened gradients by nonlinear processes and then one performs linear theory on this state. Kelley and Ott (1978) suggested that the ESF bubbles, in the collisionless R-T regime, generate a wake with vortices. They then applied two dimensional fluid turbulence theory to the model. This resulted in the development of turbulence at

shorter and longer wavelengths than the bubble size. This in turn led to a prediction of k^{-1} for the power spectrum (which does not appear to be in agreement with existing experimental observations) in the range $L_S^{-1} < k < L_D^{-1}$, where L_S is the stirring (bubble) size and L_D is a dissipation length cutoff. In a continuation of the numerical simulation work, Ossakow et al. (1978) showed a more rapid ESF development and higher bubble rise velocities resulting from sharper bottomside background electron density gradients and higher altitudes of the F peak. In Huba et al. (1978) very small scale (wavelengths $\sim$ 1m and 36cm) irregularities are reported. A two step process, utilizing high frequency ($\gtrsim \Omega_i$) kinetic drift cyclotron or lower hybrid drift instabilities, is invoked to explain them. Linear theory for these instabilities, in the ESF environment, was performed on the nonlinear state with encouraging results.

The above introductory remarks glaringly point out that much work and significant progress in the theoretical area of equatorial Spread F has been accomplished in the past few years (indeed just look at the number of publications during 1978 alone). Notwithstanding the recent successes, much work still needs to be done. Indeed, the theoretical and numerical simulation efforts in ESF are continuing along a hot and heavy path. Section II of this paper presents outlines of some of the theoretical efforts briefly mentioned in the preceding paragraphs. Given the length limitations, it would be exceedingly difficult to outline all of the theoretical works mentioned or even to present all of the details of a few works.

Section II, hopefully, will wetten the reader's appetite to read the referenced works. Section III presents a summary concerning ESF theory.

II. Theory

In this section we present some representative theoretical and numerical simulation works with the appropriate references.

a. General. The basic plasma fluid equations applicable to the equatorial Spread F ionosphere are as follows:

$$\frac{\partial n_\alpha}{\partial t} + \nabla \cdot (n_\alpha \underline{V}_\alpha) = P - \nu_R n_\alpha \tag{1}$$

$$-T_e \nabla n_e - e n_e \left(-\nabla\phi + \frac{\underline{V}_e \times \underline{B}_o}{c}\right) = 0 \tag{2}$$

$$m_i n_i \left(\frac{\partial}{\partial t} + \underline{V}_i \cdot \nabla\right) \underline{V}_i = -T_i \nabla n_i$$

$$+ e n_i \left(-\nabla\phi + \frac{\underline{V}_i \times \underline{B}_o}{c}\right) + m_i n_i \underline{g} - m_i n_i \nu_{in} \underline{V}_i \tag{3}$$

$$\nabla \cdot \underline{J} = 0 \tag{4}$$

$$\underline{J} = ne (\underline{V}_i - \underline{V}_e) \tag{5}$$

In the above equations the subscript α denotes species (e is electron, i is ion), n is density, $\underline{V}$ is velocity, P is the production, ν_R is the chemical recombination rate, T is temperature, ∇ is the gradient

operator, $\underline{B}_o$ is the ambient magnetic field (taken to be uniform), e is the electronic charge, c is the speed of light, m is mass, $\underline{g}$ is gravity, ν_{in} is the ion-neutral collision frequency, $\underline{J}$ is current, and the electrostatic approximation has been made where $\underline{E} = -\nabla\phi$. Equation (1) is the continuity equation, (2) and (3) are the electron and ion momentum equations, respectively, (4) is the divergence of the current and (5) is the current equation. What we have in mind is to apply the set of equations (1) - (5) to the two dimensions perpendicular to $\underline{B}_o$ at the geomagnetic equator, making various approximations.

Assuming a harmonic perturbation dependence of the form $\exp -i\,(\underline{k} \cdot \underline{x}_\perp - \omega t)$, where $\perp$ denotes perpendicular to $\underline{B}_o$ ($\underline{k}$ is horizontal) and linearizing equations (1) - (5) we obtain for the linear growth rate

$$\gamma = \left[-\nu_{in} + \left(\nu_{in}^2 - 4\,\underline{g} \cdot \frac{\nabla n_o}{n_o}\right)^{\frac{1}{2}}\right]/2 - \nu_R \qquad (6)$$

$$\omega \equiv \omega_r + i\gamma$$

which reduces to

$$\gamma = \begin{cases} \dfrac{g}{\nu_{in} L} - \nu_R\,, & \nu_{in}^2 \gg 4\,g/l \qquad (7a) \\[2ex] \dfrac{(g)^{\frac{1}{2}}}{L} - \nu_R\,, & \nu_{in}^2 \ll 4\,g/L \qquad (7b) \end{cases}$$

$$|L| = \left|\frac{\nabla n_o}{n_o}\right|$$

in the collision dominated and inertia dominated regimes, for $kL >> 1$. Equations (7a) and (7b) represent the R-T instability, including recombination damping, in the respective regimes. (It should be noted that this only represents instability on the bottom-side of the F region where the first term in (7a) and (7b) is positive.)

b. 2D Computer Simulation Results. In this section we will outline the two dimensional ($\perp \underline{B}_o$) computer simulation results (Scannapieco and Ossakow, 1976; Ossakow et al., 1978). The simulations follow the nonlinear evolution of the collisional R-T instability; consequently, in eqn. (3) inertial terms (i.e., the left hand side of the eqn.) are neglected. Furthermore, one takes for the F region $\nu_{in}/\Omega_i << 1$ ($\Omega_i = eB_o/m_i c$) and the quasi-neutrality assumption is made, i.e., $n_e \approx n_i \approx n$. Equations (1) - (5) then become

$$\frac{\partial n_\alpha}{\partial t} + \nabla \cdot (n_\alpha \underline{V}_\alpha) = - \nu_R (n_\alpha - n_{\alpha o}) \tag{8}$$

$$\underline{V}_e = \frac{c}{B_o} \underline{E} \times \hat{z} \tag{9}$$

$$\underline{V}_i = \left(\frac{\underline{g}}{\Omega_i} + \frac{c}{B_o} \underline{E} \right) \times \hat{z} + \frac{\nu_{in}}{\Omega_i} \left(\frac{\underline{g}}{\Omega_i} + \frac{c}{B_o} \underline{E} \right) \tag{10}$$

$$\nabla \cdot \underline{J} = 0 \ , \ \underline{J} = ne(\underline{V}_i - \underline{V}_e) \tag{11}$$

where one has taken $T_e = T_i = 0$ for simplicity (see Ossakow et al., 1978), $\underline{B}_o = B_o \hat{z}$ and the subscript o refers to equilibrium quantities.

Making the electrostatic assumption

$$\underline{E} = - \nabla\phi \tag{12}$$

and breaking the potential into an equilibrium and a perturbed quantity,

$$\phi = \phi_o + \tilde{\phi} \tag{13}$$

eqns. (8) - (11) become

$$\frac{\partial n}{\partial t} - \frac{c}{B_o}(\nabla\tilde{\phi} \times \hat{z})\nabla \cdot n = - \nu_R(n-n_o) \tag{14}$$

$$\nabla \cdot (\nu_{in} n \nabla\tilde{\phi}) = \frac{B_o}{c}(\underline{g} \times \hat{z}) \cdot \nabla n \tag{15}$$

where eqns. (14) and (15) are taken to be two dimensional ($\perp \underline{B}_o$). Linearizing eqns. (14) and (15), taking a horizontal perturbation results, as in eqn. (7a) but in a more illustrative form, in the linear growth rate

$$\gamma = - \frac{g}{\nu_{in}} \cdot \frac{\nabla n_o}{n_o} - \nu_R$$

This clearly shows that only the bottomside of the F region where ∇n_o is positive can be linearly unstable (and only if the first term $> \nu_R$).

Equations (14) and (15) were solved numerically using a vertical mesh spacing of $\Delta y = 2$ km and total y extent of 200km, and an east-west, horizontal mesh spacing $\Delta x = 200$m and a total horizontal extent of 8km. Realistic profiles of ν_{in} and ν_R as a function of

altitude were utilized. The system was initialized with a perturbation of a few percent in the horizontal (x), east-west direction with a wavelength $\sim$3km and the evolution in time of (14) and (15) was followed for different background electron density profiles. Figure 3 shows the results for a background electron density, n_o, profile with an F peak at 354km and a minimum bottomside background electron density gradient scale length, L $\sim$10km. In this case at t = 4000 sec a bubble (plasma density depletion) is clearly forming and beginning to rise in the central portion of the mesh (note $n \equiv n_o + n_1$). The isodensity contours are such that the maximum absolute value of the enhancement or depletion is in the center and the contours decrease (in absolute percentage) as one goes toward the outer contours. At t = 4000 sec the maximum depletion within the bubble is 54% and the maximum enhancement over the mesh is 84%. At t = 8000 sec we notice that the bubble has reached the altitude of the F peak, with the innermost contour of the rising bubble representing a 41% depletion. At $t = 10^4$ sec the main bubble is clearly through the F peak with an innermost depletion contour of 41%. However, in the ionosphere below the bubble near x = 0 there is a 71% depletion contour, similarly in the wings near $|x|$ = 4km. The innermost enhancement contour, at this time, represents a 236% enhancement with a maximum inside this contour of 294%. Note that the top of the main bubble is at an altitude of 375km while the bottom trail of the bubble is at an altitude of 270km. Between t = 8000 and 10^4 sec the bubble has risen $\sim$24km which represents a rise velocity $\sim$12m/sec.

Also note that the bubble is ∿1km wide. Figure 4 depicts contours of constant induced potential ϕ_1 at t = 10^4 sec. This shows that the more isolated part of the high altitude bubble depicted in Fig. 3 is acted on by an induced electric field which points from west to east and is dipolar in nature. This causes the bubble to rise with a $(-c/B_o)\nabla \phi_1 \times \hat{z}$ velocity. However, the lower portion of the mesh is acted on by an induced electric field which points from east to west. This field is much weaker than the induced field acting on the isolated portion of the central bubble. The lower altitude electric field causes the enhancements and depletions to move downward. Thus, the lower altitude portion of the central bubble becomes captured by the enhancements.

Figure 5 presents for comparison a case in which the background electron density profile (shape) was kept the same, but the entire profile moved up in altitude so that the F peak was at 434km. All other parameters are the same as in Figure 3, except ν_{in} and ν_R are taken for the altitude range 332km to 532km (those used in this simulation). One can immediately note the more rapid time evolution of the Spread F process with respect to that presented in Fig. 3. At t = 700 sec, a rising bubble with an innermost contour of 79% and a maximum depletion inside this contour of 84% were noted. At t = 1000 sec the bubble has reached the peak and at this time the innermost depletion contour is 85%. The long trail associated with the high altitude bubble has a 100km extension to lower altitudes. At t = 1400 sec the top of the main bubble is at an altitude ∿500km

and has a long trail connecting to an altitude of 357km. There is a maximum 70% depletion within the innermost contour of the high altitude bubble. Between t = 10^3 and 1400 sec the top part of the bubble rose ∿65km and this represents a rise velocity ∿160m/sec. Potential contour results for this simulation show similar patterns to those exhibited in Fig. 4. Naturally, the induced electric fields causing the bubble to rise in the present case are stronger. This spread in bubble rise velocities has been observed by AE satellite data (McClure et al., 1977).

Other numerical simulations in this series have been performed and the paper by Ossakow et al. (1978) should be consulted for more details. The basic conclusions reached from these simulations are as follows: (i) the collisional R-T instability causes linear growth on the bottomside of the equatorial Spread F region; (ii) plasma density depletions (bubbles) steepen on their top and nonlinearly rise to the topside ionosphere, beyond the F peak, by polarization (induced) $\underline{E} \times \underline{B}$ forces; and (iii) high altitude of the F peak, small bottomside background electron density gradient scale lengths, and large percentage depletions yield large vertical bubble rise velocities, with the first two conditions favoring collisional R-T linear growth (instability). In addition, large spatial bubbles with similar rise velocities to those presented here, but with almost 100% depletions, have been produced by numerical simulations (Zalesak et al., 1978). In these cases the horizontal mesh covered 200km in extent (intermesh spacing Δx = 5km) and a long wavelength (∿75km) initial perturbation was

used. Bubbles with horizontal dimensions ∿50km resulted. The NRL group has also added neutral wind effects to these simulations and found that an eastward neutral wind results in a westward motion of the bubbles in addition to its rise. This is also in agreement with observations of bubble motion (see McClure et al., 1977).

c. Analytical 2D Coherent Mode Coupling Results. A two dimensional nonlinear quasi-final state of the collisional R-T instability was investigated by Chaturvedi and Ossakow (1977) using analytical means and considering coherent mode coupling as the saturation mechanism. Equations (14) and (15) were utilized with $n = n_o + \tilde{n}$, etc. This yields the following coupled nonlinear equations

$$\frac{\partial \tilde{n}}{\partial t} - \frac{c}{B_o} \nabla\tilde{\phi} \times \hat{z} \cdot \nabla n_o = - \nu_R \tilde{n} + \frac{c}{B_o} \nabla\tilde{\phi} \times \hat{z} \cdot \nabla\tilde{n} \qquad (16)$$

$$\frac{\underline{g}\times\hat{z}}{\Omega_i} \cdot \nabla\tilde{n} - \frac{c}{B_o \Omega_i} \left[n\nu_{in} \nabla^2\tilde{\phi} + \nabla\tilde{\phi} \cdot \nabla(\tilde{n}\nu_{in}) \right] = 0 \qquad (17)$$

where the second term on the LHS of (16) represents growth, the first term on the RHS represents damping, and the second term on the RHS is the nonlinear term. Comparing the nonlinear term in (16) with the last term in (17) results in

$$\frac{c}{B_o} \nabla\tilde{\phi} \times \hat{z} \cdot \nabla\tilde{n} : \frac{c}{B_o \Omega_i} \nabla\tilde{\phi} \cdot \nabla(\tilde{n}\nu_{in}) \approx \frac{\Omega_i}{\nu_{in}} \quad >> 1$$

Therefore, eqn. (17) is treated linearly and the nonlinearity is retained in (16). A perturbation of the form

$$\frac{\tilde{n}}{n_o} = A_{1,1} \sin (k_y y - \omega t) \cos k_x x + A_{2,0} \sin 2k_x x \qquad (18)$$

is chosen. In this analysis x is vertical (altitude) and y horizontal (east-west). This is the way it appears in the reference. For the convenience of the reader, in referring to the original work, we have kept the coordinate system of the reference.

The coupled mode equations for the amplitudes $A_{1,1}$ and $A_{2,0}$ become

$$\frac{\partial A_{1,1}}{\partial t} = \gamma_{1,1} A_{1,1} - 2\alpha A_{1,1} A_{2,0} \qquad (19)$$

$$\frac{\partial A_{2,0}}{\partial t} = \gamma_{2,0} A_{2,0} + \frac{\alpha}{2} A_{1,1}^2 \qquad (20)$$

where the coupling coefficient $\alpha = k_x k_y^2 g/k^2 \nu_{in}$, and $\omega \equiv \omega_r + i\gamma$. It should be noted that the linear growth rate $\gamma_{2,0}$ is negative, i.e., the purely vertical mode $A_{2,0}$ is linearly damped. Also $\gamma_{1,1}$ is positive and represents linear growth of the mode $A_{1,1}$. In the saturated steady state one has $\partial A_{1,1}/\partial t = \partial A_{2,0}/\partial t = 0$ and from (19) and (20) this results in

$$A_{2,0} = \frac{\gamma_{1,1}}{2} \approx \frac{1}{2 k_x L} \qquad (21)$$

$$A_{1,1} \approx \left(\frac{k^2}{k_y^2} \frac{\nu_R \nu_{in}}{g L k_x^2} \right)^{1/2} \approx \left(\frac{-2\gamma_{2,0}}{\alpha} A_{2,0} \right)^{1/2} \qquad (22)$$

For typical values of the parameters, $A_{2,0} >> A_{1,1}$ and shows $A_{2,0} \propto k_x^{-1}$ (i.e., the power spectrum would $\propto k_x^{-2}$). This represents a coherent nonlinear evolution where the linearly damped mode $A_{2,0}$ is generated nonlinearly by the linearly unstable mode $A_{1,1}$, by a harmonic generation ($A_{1,1}$ contains k_x and $A_{2,0}$ contains $2k_x$). More detailed information can be found in Chaturvedi and Ossakow (1977).

d. Analytical Models for ESF Bubbles. First we will discuss collisional R-T bubbles (Ossakow and Chaturvedi, 1978) in which the electrical analogy with plasma density enhancement (e.g., barium clouds) was utilized and results obtained for general 2D ($\perp \underline{B}_o$) bubble shapes. Here eqns. (14) and (15) are utilized with the further simplifying assumptions of neglecting recombination chemistry ($\nu_R = 0$) and the explicit altitude dependence of the ion-neutral collision frequency, ν_{in}. The following set of equations result.

$$\frac{\partial n}{\partial t} - \frac{c}{B_o}(\nabla\tilde{\phi} \times \hat{z}) \cdot \nabla n = 0 \tag{23}$$

$$\nabla \cdot (n\nabla\tilde{\phi}) = \underline{E}^* \cdot \nabla n \tag{24}$$

$$\underline{E}^* = \underline{E}_o + \frac{\Omega_i}{\nu_{in}} \frac{m_i}{e} \underline{g} \times \hat{z} \tag{25}$$

where an ambient horizontal electric field $\underline{E}_o$ has been included to show more generality. Equation (24) can be thought of, in general, as a potential equation for a dielectric immersed in the applied electric field, $\underline{E}^*$. The plasma density depletion (bubble) is analogous to the case of a cavity immersed in a dielectric with a

uniform electric field ($\underline{E}^*$). In general (23) and (24) do not admit of a two dimensional ($\perp B_o$), steady state solution. However, for the case of a constant density inside the depletion and a constant density outside the depletion, two dimensional steady state solutions can be obtained.

For a constant density depletion with an elliptical shape one has

$$n(x,y) = n_o - n_D(x,y)$$

$$= n_o \left[1 - \frac{\delta n}{n_o} F(x,y)\right] \tag{26}$$

$$n_D = \delta n \, H\left[1 - \left(\frac{x}{a}\right)^2 - \left(\frac{y}{b}\right)^2\right] \tag{27}$$

$$H(x) = \begin{cases} 1, & x > 0 \\ 0, & x < 0 \end{cases}$$

where H is the Heaviside function (note the geometry is taken such that x is vertical and y horizontal). For this elliptical shape, the solution to (24), neglecting $\underline{E}_o$, is

$$\frac{\partial \tilde{\phi}}{\partial y} = - \frac{\Omega_i}{\nu_{in}} \frac{m_i g}{e} \left(\frac{a \qquad \delta n/n_o}{b + a(1 - \delta n/n_o)} \right) \tag{28}$$

Using $-(c/B_o)\ \nabla\tilde{\phi} \times \hat{z}$ this further results in the nonlinear vertical bubble rise velocity, V_B, given by

$$V_B = \frac{g}{\nu_{in}} \left(\frac{a \qquad \delta n/n_o}{b + a(1 - \delta n/n_o)} \right) \tag{29}$$

Limiting cases of (29) for sheet, cylindrical and slab bubble

geometries are given by

$$\frac{V_B}{g/\nu_{in}} = \begin{cases} (\delta n/n_o)\ (1 - \delta n/n_o)^{-1}, & b \ll a \quad (30a) \\ (\delta n/n_o)\ (2 - \delta n/n_o)^{-1}, & b = a \quad (30b) \\ 0, & b \ll a \quad (30c) \end{cases}$$

For typical values of ν_{in} as a function of altitude, Fig. 6 exhibits rise velocities given by (30b) for various percentage depletions. Table 1 shows the rise velocities, in units of g/ν_{in}, for various shapes. (Note that the linear case comes from linearizing (23) and (24)). All of the geometry results can be expressed in a concise formula

$$V_B = \frac{g}{\nu_{in}} f\left(\frac{\delta n}{n_o}\right) \quad (31)$$

where $f(\delta n/n_o)$ is an increasing function of the percentage depletion $\delta n/n_o$. Basically, the results predict that high altitudes and/or large percentage depletions yield high vertical rise velocities for the bubbles (in agreement with experimental observations).

Collisional and collisionless (inertia dominated) two dimensional cylindrical R-T bubbles have been studied analytically by Ott (1978). This study is based on the analogy with fluid dynamic flows and brings forth some of the work done on two-dimensional fluids. This study begins with the basic equations (1) - (3), considers two dimensions ($\perp \underline{B}_o$), sets $n_e \approx n_i \approx n$, and makes the assumption that

$$\Omega_i >> \frac{\partial}{\partial t}, \underline{V}_i \cdot \nabla, \nu_{in} \quad (31)$$

To lowest order, using (31), one obtains from (3) a lqwest order ion

velocity (with $\hat{z} = \underline{B}_o/|\underline{B}_o|$),

$$\underline{V}_i^{(o)} = \frac{\hat{z} \times \nabla\phi}{B_o} + \frac{\hat{z} \times \nabla p_i}{neB_o} + \frac{m_i \underline{g} \times \underline{B}_o}{eB_o^2} \tag{32}$$

(Note that mks units are being used here to coincide with the units used by Ott (1978)). Quasi-neutrality, i.e., $\nabla \cdot \underline{J} = 0$, with the assumption of two dimensionality implies that $\underline{J}$ can be specified in terms of a single scalar potential function, ψ, such that

$$\underline{J} = - \hat{z} \times \nabla\psi \tag{33}$$

Using eqn. (2) for the electron velocity, and a next order ion velocity equation obtained by putting (32) into (3), the following ion velocity equation is obtained

$$nm_i \left[\frac{\partial \underline{V}_i^{(o)}}{\partial t} + \underline{V}_i^{(o)} \cdot \nabla \right] \underline{V}_i^{(o)} = - \nabla \tilde{p} - nm_i \nu_{in} \underline{V}_i^{(o)} + nm_i \underline{g} \tag{34}$$

with $\tilde{p} = p_e + p_i + B\psi$. Using (32) and the assumption of either isothermal or adiabatic ions one has

$$\nabla \cdot \underline{V}_i^{(o)} = 0 \tag{35}$$

Using $\underline{V}_i^{(o)}$ in the ion continuity equation (1) with $\nu_R = P = 0$, eqn. (1) becomes

$$\frac{\partial n}{\partial t} + \underline{V}_i^{(o)} \cdot \nabla n = 0. \tag{36}$$

Equations (34) - (36) form a complete set of equations sufficient to determine the unknown quantities $\underline{V}_i^{(o)}$, n, and $\tilde{p}$. In the limit of $\nu_{in} \to 0$, eqns. (34) - (36) are identical to those of an ideal incompressible fluid. At this point the philosophy taken is that there is much to be learned concerning bubbles in the ESF ionosphere from the extensive studies of bubbles in fluids. One then uses a stream function ξ such that

$$\underline{V}_i^{(o)} \equiv \hat{z} \times \nabla \xi \tag{37}$$

After a series of manipulations one can obtain an equation for the stream function. In the collisional and collisionless case one finds that for certain values of the bubble rise velocity ξ will satisfy the equation, for a cylindrical shape (see Ott, 1978 for more details).

The results of this study by Ott (1978) predicts the bubbles to be cylindrical (circular cap at top) in two dimensions. The bubble rise velocity in the collision-dominated regime, for a 100% depletion, is given by

$$V_B = \frac{g}{\nu_{in}} \tag{38}$$

which is altitude dependent. This result is the same as that predicted by (30b) for $\delta n/n_o = 1$, i.e., a 100% depletion. In the inertia (collisionless) dominated regime, for a 100% depletion, the bubble rise velocity is given by

$$V_B \simeq \tfrac{1}{2} (Rg)^{\frac{1}{2}} \tag{39}$$

where R is the radius of curvature at the top of the bubble so that (39) is size dependent.

e. Analytical Work on the Very Small Scale ($\leq$10m) Irregularities. The work in this section represents essentially multilinear calculations using kinetic theory resulting in plasma kinetic drift wave modes. It is multilinear because it depends on say a two-step process whereby linear theory is performed on the non-linear state. The driving density gradients, in these calculations, are thought to arise through a primary instability, driven by the zero order background ionospheric equatorial F region electron density gradient, achieving a large amplitude state. The zero order ionospheric electron density gradient is of larger scale size than the primary instability electron density gradient scale size, which would be of the order of the instability wavelength. Because the calculations are kinetic, they employ particle distribution functions. Kinetic drift waves have been investigated for laboratory plasma fusion conditions for over twenty years, so a well developed formalism exists.

Before proceeding with specific calculations let us present some general concepts regarding kinetic drift waves which will be useful for both types of calculations presented in this section. The basic geometry is such that

$$\underline{B} = \underline{B}_o \hat{z} \tag{40a}$$

$$n_o = n_o(x) \tag{40b}$$

(similar to the zero order background equatorial ionospheric geometry) where here $n_o(x)$ arises due to the primary instability. The orthogonal coordinate system is completed by the ion and electron diamagnetic velocities being along the y axis,

$$\underline{V}_d = (V_{di} - V_{de})\ \hat{y} \tag{41a}$$

$$V_{di} = (V_i^2/2\Omega_i)\ (\partial \ln n_o/\partial x) \tag{41b}$$

$$V_{de} = -\ (V_e^2/2\Omega_e)\ (\partial \ln n_o/\partial x) \tag{41c}$$

where $V_{i,e} = (2T_{i,e}/m_{i,e})^{\frac{1}{2}}$ and the larmor radius is defined by $r_\alpha = V_\alpha/\Omega_\alpha$. The linear analysis is then performed with this in mind.

First the low frequency ($\omega << \Omega_i$) collisionless drift wave calculations of Costa and Kelley (1978a,b), for $kr_i \sim 1$ (r_i is the ion gyroradius), will be presented. These calculations were meant to provide a basis within which to try and account for the 3 meter radar backscatter observations of Jicamarca (see Woodman and La Hoz, 1976). A linear kinetic dispersion relation is derived using perturbations of the form $\exp i\left[\underline{k} \cdot \underline{x} - \omega t\right]$, where $\underline{k} = k_\parallel \hat{z} + k_\perp \hat{y}$ and $\omega = \omega_r + i\gamma$. Furthermore, assumptions are made such that $\omega << \Omega_i$, $V_i << |\omega/k_\parallel| << V_e$ and $\omega > \nu_{in}$, ν_{ie}, ν_{ii}, which are the ion-neutral, ion-electron, and ion-ion collision frequencies, respectively. This analysis depends on having a $k_\parallel$, a component of the wavevector along the ambient geomagnetic field. Figure 7 shows some growth rate results from these calculations. The growth rate is in units of the ion thermal velocity

divided by the electron density gradient scale length ($L = n_o (dn_o/dx)^{-1}$). Figure 8 depicts some measured inverse electron density gradient scale lengths during ESF and maximum growth rates as a function of these inverse scale lengths. The basic results of these calculations show maximum growth for $k_\perp r_i \approx 1.5$, i.e., $\lambda_\perp \approx 20$m (for typical ESF parameters) with growth rates $\gtrsim 1$ sec^{-1}. For more detailed analysis concerning these low frequency drift waves applied to ESF see Costa and Kelley (1978a,b).

Now we present the high frequency drift wave analysis of Huba et al. (1978). In this reference radar backscatter observed irregularities with wavelengths of 1 meter and 36 cm at Kwajalein during ESF conditions are shown. In an effort to explain these very short wavelength irregularities high frequency ($\omega \gtrsim \Omega_i$) drift waves were analyzed for ESF conditions. These waves are the so-called drift cyclotron (DC) or lower hybrid drift (LHD) instabilities with maximum growth rates for $k_\perp r_e \sim 1$ (and $k_\parallel = 0$). No $k_\parallel$ is required for these instabilities. The parameter determining which instability operates in a collisional plasma is

$$C_f = (\nu_{ii}/\Omega_i)\ (k_\perp r_i)^2 \tag{42}$$

Utilizing the linear dispersion relation for high frequency drift waves for $C_f << 1$, instability results for

$$L/r_i < (1/2\ell)\ (m_i/m_e)^{\frac{1}{2}} \tag{43}$$

where ℓ is the harmonic number ($\omega_r \approx \ell\Omega_i$). For the 0^+ ESF ionospheric plasma this requires the electron density gradient scale length

$L < 340m$, which is satisfied (see Fig. 8). Growth rates for these instabilities are given by

$$\gamma \approx (m_e/m_i)^{1/4} \ell \Omega_i \tag{44}$$

However, the condition $C_f << 1$ implies that $(k_\perp r_i)^2 n << 2 \times 10^7$ and for $k_\perp r_e \sim 1$ this means $n << 10^3$ cm^{-3}, which is quite restrictive. Longer wavelengths, i.e., smaller values of $k_\perp r_e$ would raise the density restriction somewhat, but still be restrictive for ESF conditions.

For $C_f \gtrsim 1$, the lower hybrid drift instability is operative and there is no threshhold condition on L. Basically, the collisions which increase C_f destroy the ion gyroresonances needed for the DC instability to operate. The real and imaginary part of the frequency for the LHD instability are given by

$$\frac{\omega_r}{\Omega_i} \sim \frac{r_i}{L}\left(\frac{m_i}{m_e}\right)^{1/2}, \frac{\gamma}{\Omega_i} \sim \left(\frac{r_i}{L}\right)^2 \left(\frac{m_i}{m_e}\right)^{1/2} \tag{45}$$

In the collisionless limit it should be noted that the DC instability transforms into the LHD instability for high enough ion diamagnetic velocities such that

$$L/r_i \lesssim (m_i/m_e)^{1/4}$$

which for ESF conditions implies that $L \lesssim 30m$. Figures 9 and 10 show some typical results from the analysis of the high frequency drift wave linear dispersion relation.

The results of this analysis predicts that the lower hybrid drift instability is dominant for most typical ESF ionospheric parameters. Also, maximum growth of the instability occurs for $k_\perp r_e \sim 1$ ($\lambda_\perp \sim 21$ cm), although good growth rates can occur for $\lambda_\perp \sim 1$ m. Finally, from this instability, large growth rates ($\gamma \lesssim \Omega_i$) resulting in growth times, $\tau = \gamma^{-1}$, less than a second can occur. For more details of this work see Huba et al. (1978).

III. Summary

Although much progress has been made in the theoretical efforts directed toward the equatorial Spread F ionosphere, especially in the past three years, more has to be done. Also the burden cannot be placed on the theoretician alone. Correlative measurements have to be made prior to and during ESF conditions. It is not sufficient to make a single measurement with one instrument and then expect a complete theoretical description of ESF. One needs to know the state of the ionosphere with respect to driving parameters such as background electron density profiles (bottomside electron density gradient scale lengths and height of the F peak), d.c. electric fields, neutral winds, and ionic mass composition in order to build a predictive model. In addition, in order to compare results from the predictive model, measurements of the in situ fluctuating component of the electric field and plasma density have to be made, as well as radar backscatter measurements of the very small scale irregularities ($\lesssim$ 10m) and ground measurements of satellite signal propagation amplitude and phase scintillations.

Some of the remaining theoretical problems could be listed as follows. (1) What are the effects of changing initial conditions, including ion inertia, and including neutral winds in the numerical simulations? (2) An analytical description of many bubbles rising. (3) How do bubbles decay and what role does diffusion, etc. play? (4) How does a turbulent development occur? (5) What are the effects of other regions of the ionosphere (e.g., E region) on ESF? (6) A more complete study of collisional effects on drift waves is needed. What determines when the small scale irregularities should occur (a more quantitative description)? (7) A determination of the nonlinear saturation of small scale irregularities (instabilities) is needed. (8) What are the effects of $k_{\parallel}$? Indeed points (6) and (7) are tied to the more general question of what is the relation between the very small scale ($\lesssim$10m) irregularities (which radar backscatter observes) and the longer wavelength fluid type (e.g., R-T) irregularities (which are primarily responsible for Spread F seen on ionograms)? I am sure that some more questions and points could be raised. However, the above list should keep the theoreticians busy for a reasonable time.

Acknowledgements

The author is grateful to the dedication of his colleagues in their efforts to provide an understanding of equatorial Spread F. In particular, I am deeply indebted to Pradeep Chaturvedi, Joe Huba, Mike Keskinen, Ed McDonald, Tony Scannapieco, and Steve Zalesak whose interest and work in ionospheric irregularities is the sine qua non without which this article could not have been written. In addition, this work was supported by the Defense Nuclear Agency and the Office of Naval Research.

References

Balsley, B. B., G. Haerendel and R. A. Greenwald, Equatorial Spread F: Recent observations and a new interpretation, J. Geophys. Res., 77, 5625, 1972.

Booker, B. B., and H. W. Wells, Scattering of radio waves by the F region of the ionosphere, Terres. Magn., 43, 249, 1938.

Calvert, W., Instability of the equatorial F layer after sunset, J. Geophys. Res., 68, 2591, 1963.

Chaturvedi, P., and P. Kaw, An interpretation for the power spectrum of Spread F irregularities, J. Geophys. Res., 81, 3257, 1976.

Chaturvedi, P. K., and S. L. Ossakow, Nonlinear theory of the collisional Rayleigh-Taylor instability in equatorial Spread F, Geophys. Res. Letts., 4, 558, 1977.

Costa, E., and M. C. Kelley, On the role of steepened structures and drift waves in equatorial Spread F, J. Geophys. Res., 83, 4359, 1978a.

Costa, E., and M. C. Kelley, Linear theory for the collisionless drift wave instability with wavelengths near the ion gyroradius, J. Geophys. Res., 83, 4365, 1978b.

Dagg, M., The origin of the ionospheric irregularities responsible for radio-star scintillations and spread F, 2, Turbulent motion in the dynamo region, J. Atmos. Terres. Phys., 11, 139, 1957.

Dungey, J. W., Convective diffusion in the equatorial F region, J. Atmos. Terres. Phys., 9, 304, 1956.

Dyson, P. L., J. P. McClure and W. B. Hanson, In situ measurements of the spectral characteristics of ionospheric irregularities, J. Geophys. Res., 79, 1497, 1974.

Farley, D. T., B. B. Balsley, R. F. Woodman, and J. P. McClure, Equatorial Spread F: Implications of VHF radar observations, J. Geophys. Res., 75, 7199, 1970.

Haerendel, G., Theory of Equatorial Spread F, preprint, Max-Planck Institute fur Physik und Astrophysik, Garching, West Germany, 1974.

Huba, J. D., P. K. Chaturvedi, S. L. Ossakow, and D. M. Towle, High frequency drift waves with wavelengths below the ion gyroradius in equatorial Spread F, Geophys. Res. Letts., 5, 695, 1978.

Hudson, M. K., Spread F bubbles: Nonlinear Rayleigh-Taylor mode in two dimensions, J. Geophys. Res., 83, 3189, 1978.

Hudson, M. K., C. F. Kennel, and P. K. Kaw, A two-step drift mode theory of equatorial Spread F, Trans. Am. Geophys. Un., 54, 1147, 1973.

Hudson, M. K., and C. F. Kennel, Linear theory of equatorial Spread F, J. Geophys. Res., 80, 4581, 1975.

Kelley, M. C., G. Haerendel, H. Kappler, A. Valenzuela, B. B. Balsley, D. A. Carter, W. L. Ecklund, C. W. Carlson, B. Hausler, and R. Torbert, Evidence for a Rayleigh-Taylor type instability and upwelling of depleted density regions during equatorial Spread F, Geophys. Res. Letts., 3, 448, 1976.

Kelley, M. C., and E. Ott, Two-dimensional turbulence in equatorial Spread F, J. Geophys. Res., 83, 4369, 1978.

Martyn, D. F., Large-scale movements of ionization in the ionosphere, J. Geophys. Res.,64, 2178, 1959.

McClure, J. P., W. B. Hanson, and J. H. Hoffman, Plasma bubbles and irregularities in the equatorial ionosphere, J. Geophys. Res., 82, 2650, 1977.

Morse, F. A., B. C. Edgar, H. C. Koons, C. J. Rice, W. J. Heikkila, J. H. Hoffman, B. A. Tinsley, J. D. Winningham, A. B. Christensen, R. F. Woodman, J. Pomalaza, and N. R. Teixeira, Equion, an equatorial ionospheric irregularity experiment, J. Geophys. Res., 82, 578, 1977.

Ossakow, S. L., and P. K. Chaturvedi, Morphological studies of rising equatorial Spread F bubbles, J. Geophys. Res., 83, 2085, 1978.

Ossakow, S. L., S. T. Zalesak, B. E. McDonald, and P. K. Chaturvedi, Nonlinear equatorial Spread F: Dependence on altitude of the F peak and bottomside background electron density gradient scale length, J. Geophys. Res. (in press 1978).

Ott, E., Theory of Rayleigh-Taylor bubbles in the equatorial ionosphere, J. Geophys. Res., 83, 2066, 1978.

Scannapieco, A. J., and S. L. Ossakow, Nonlinear equatorial Spread F, Geophys. Res. Letts., 3, 451, 1976.

Sudan, R. N., J. Akinrimisi, and D. T. Farley, Generation of small-scale irregularities in the equatorial electrojet, J. Geophys. Res., 78, 240, 1973.

Woodman, R. F., and C. La Hoz, Radar observations of F-region equatorial irregularities, J. Geophys. Res., 81, 5447, 1976.

Zalesak, S. T., S. L. Ossakow, B. E. McDonald, and P. K. Chaturvedi, Spatially large equatorial Spread F bubbles, Trans. Am. Geophys. Un., 59, 345, 1978.

Table I - Bubble rise velocity (in units of g/v_{in}), V'_B, as a function of fractional depleted density, $\delta n/n_o$, for various bubble shapes

V'_B \ $\frac{\delta n}{n_o}$	.25	.5	.75	.9	1
Linear	.25	.5	.75	.9	1
Sheet	.33	1	3	9	∞
Cylindrical	.14	.33	.6	.82	1
Elliptical (5:1)	.26	.71	1.67	3	5
Elliptical (10:1)	.29	.83	2.14	4.5	10

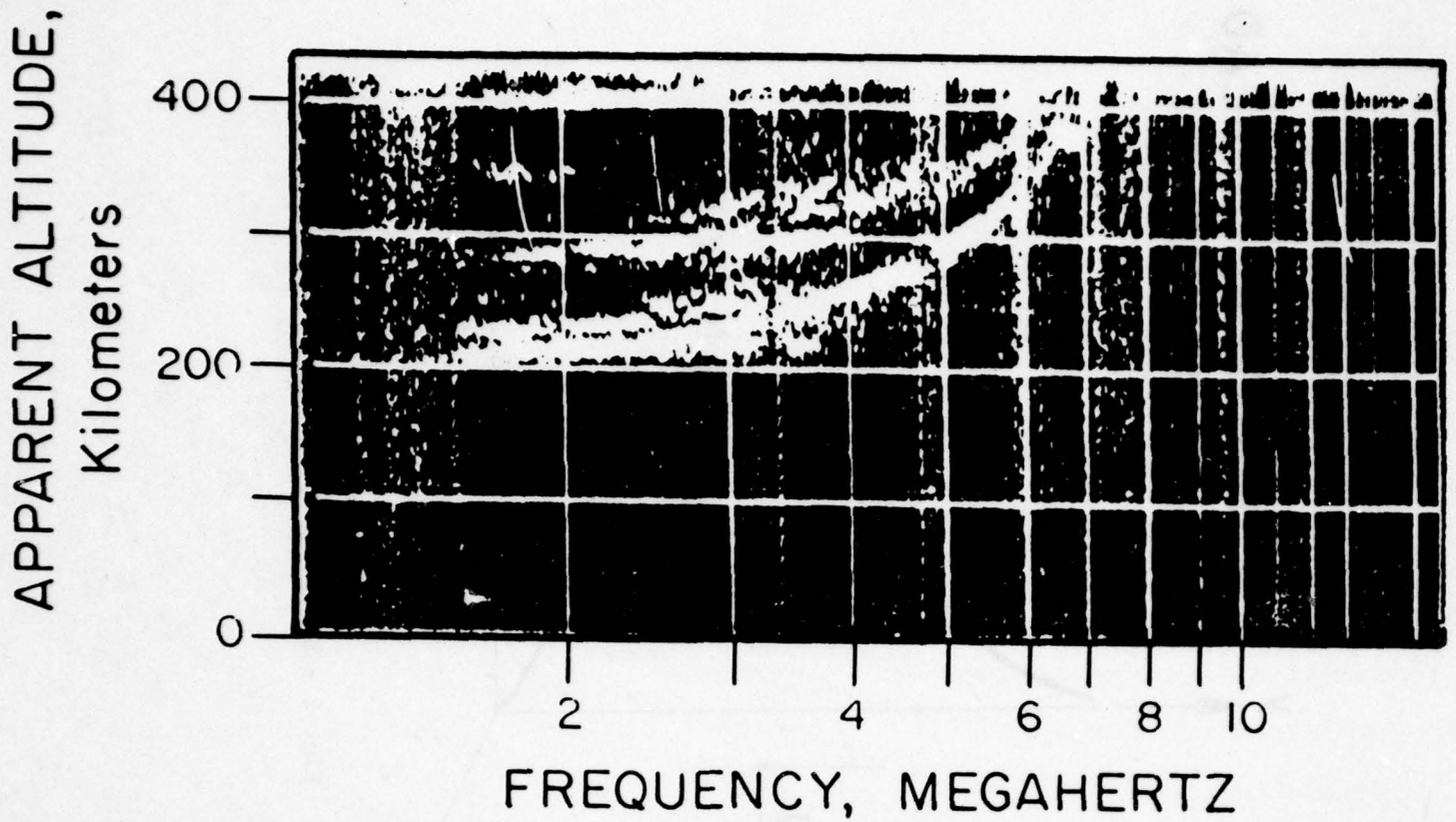

Fig. 1 - Ionogram recorded at Natal, Brazil (equatorial station), on November 18, 1973 at 2122-2123 UT. This figure was taken from Hudson and Kennel (1975)

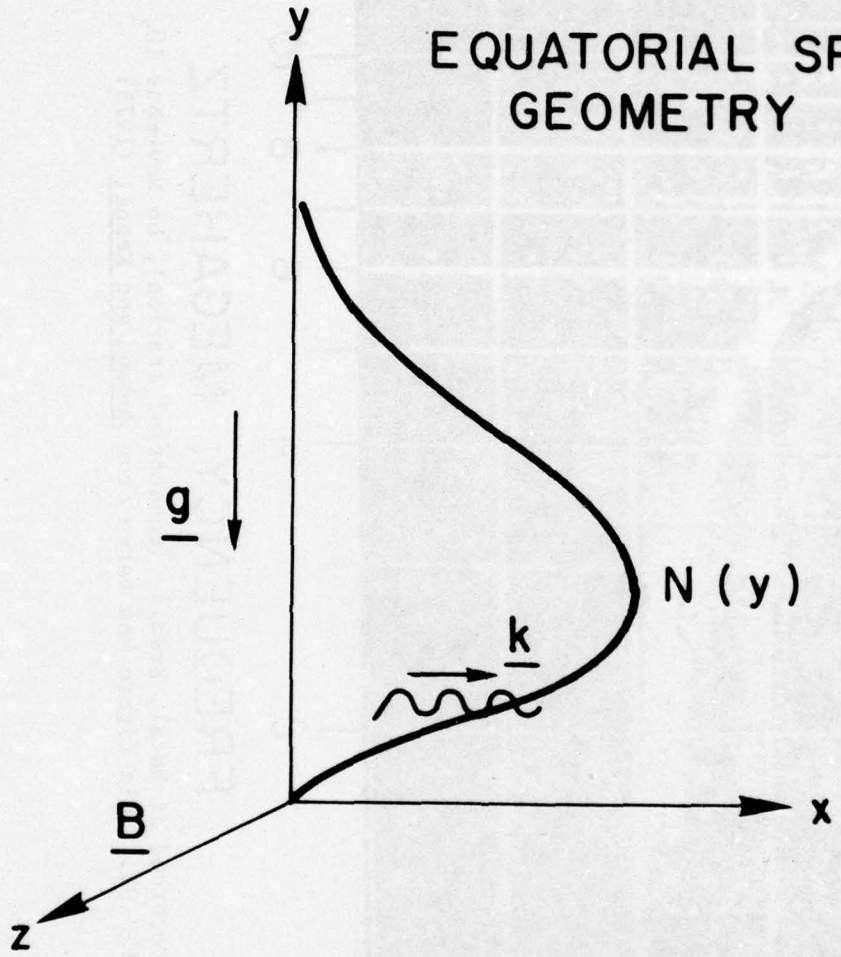

Fig. 2 - Basic equatorial Spread F geometry

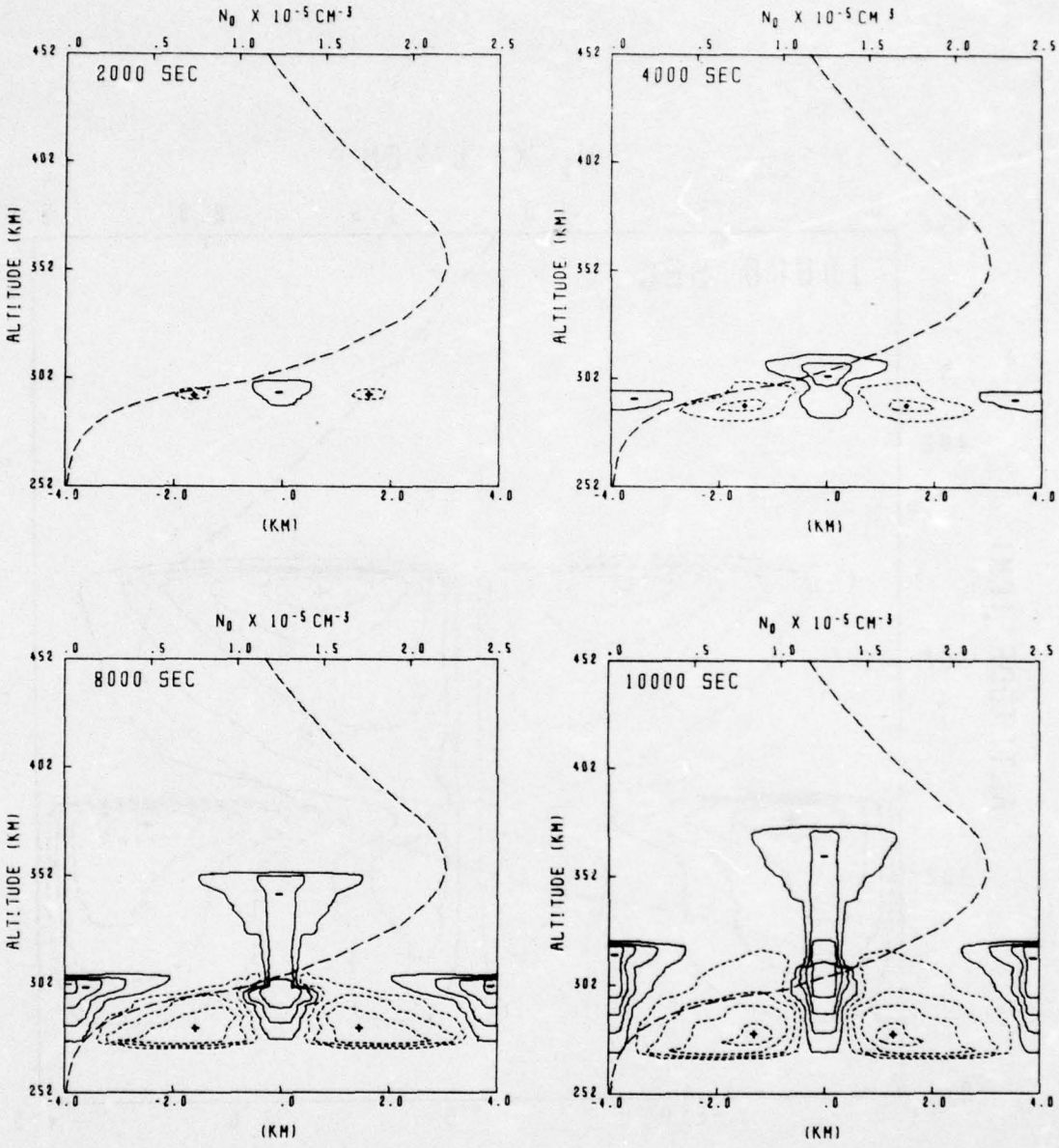

Fig. 3 - Contour plots of constant n_1/n_o for the simulation with an F peak at 354km at t = 2000, 4000, 8000, and 10,000 sec. The small dashed contours with a plus sign inside and the solid contours with a minus sign inside indicate enhancement and depletions over the ambient electron number density. The large dashed curve depicts the ambient electron number density (values on upper horizontal axis), n_o, as a function of altitude. The vertical y axis represents altitude, the lower horizontal x axis is east-west range, and the ambient magnetic field is along the z axis, out of the figure. Taken from Ossakow et al. (1978)

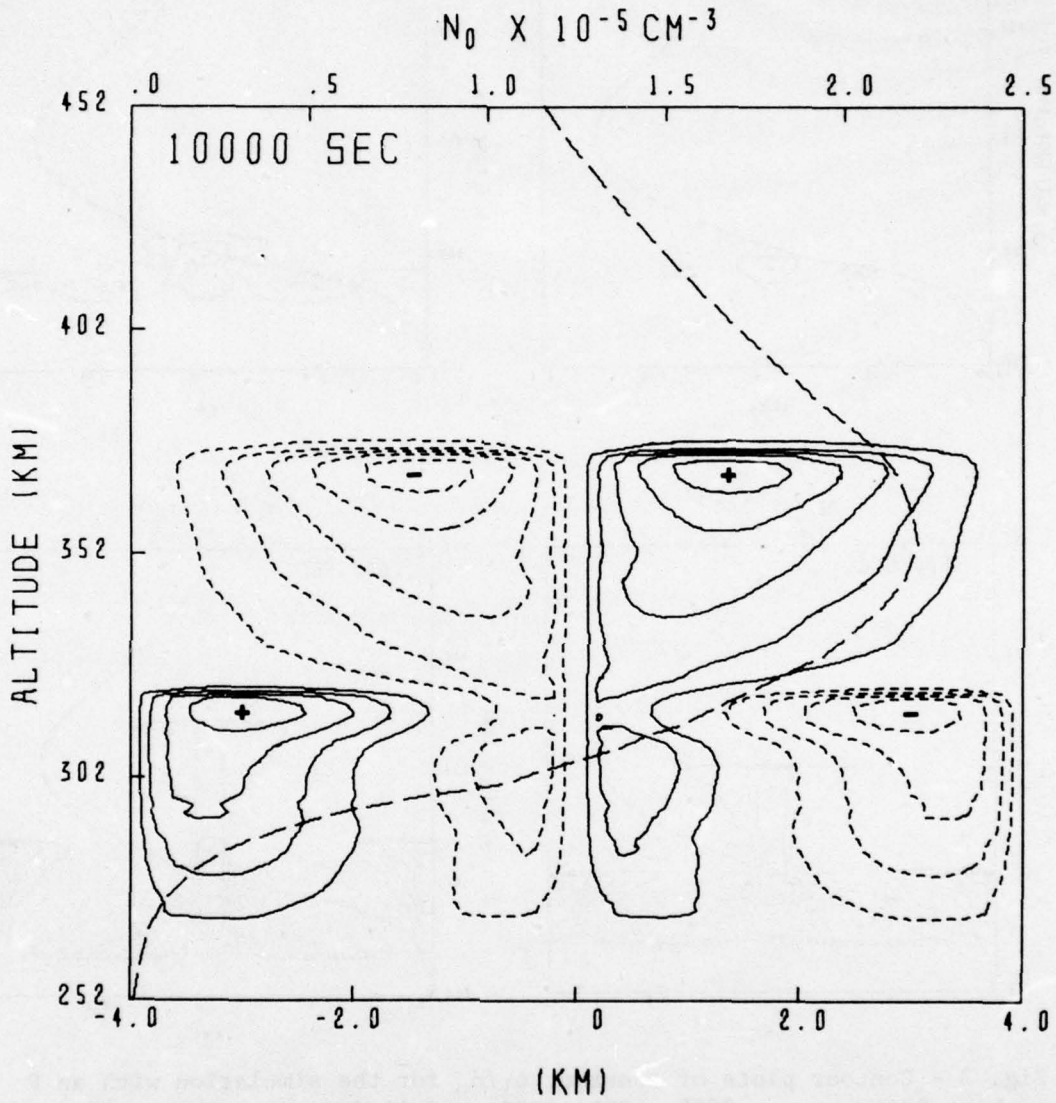

Fig. 4 - Contours of constant induced (polarization) potential, ϕ_1, over the mesh (see Fig. 3) at t = 10,000 sec. Plus and minus denote positive and negative values, with values decreasing in magnitude as one goes from the innermost to the outermost contours. The large dashed curve is n_o. Taken from Ossakow et al. (1978)

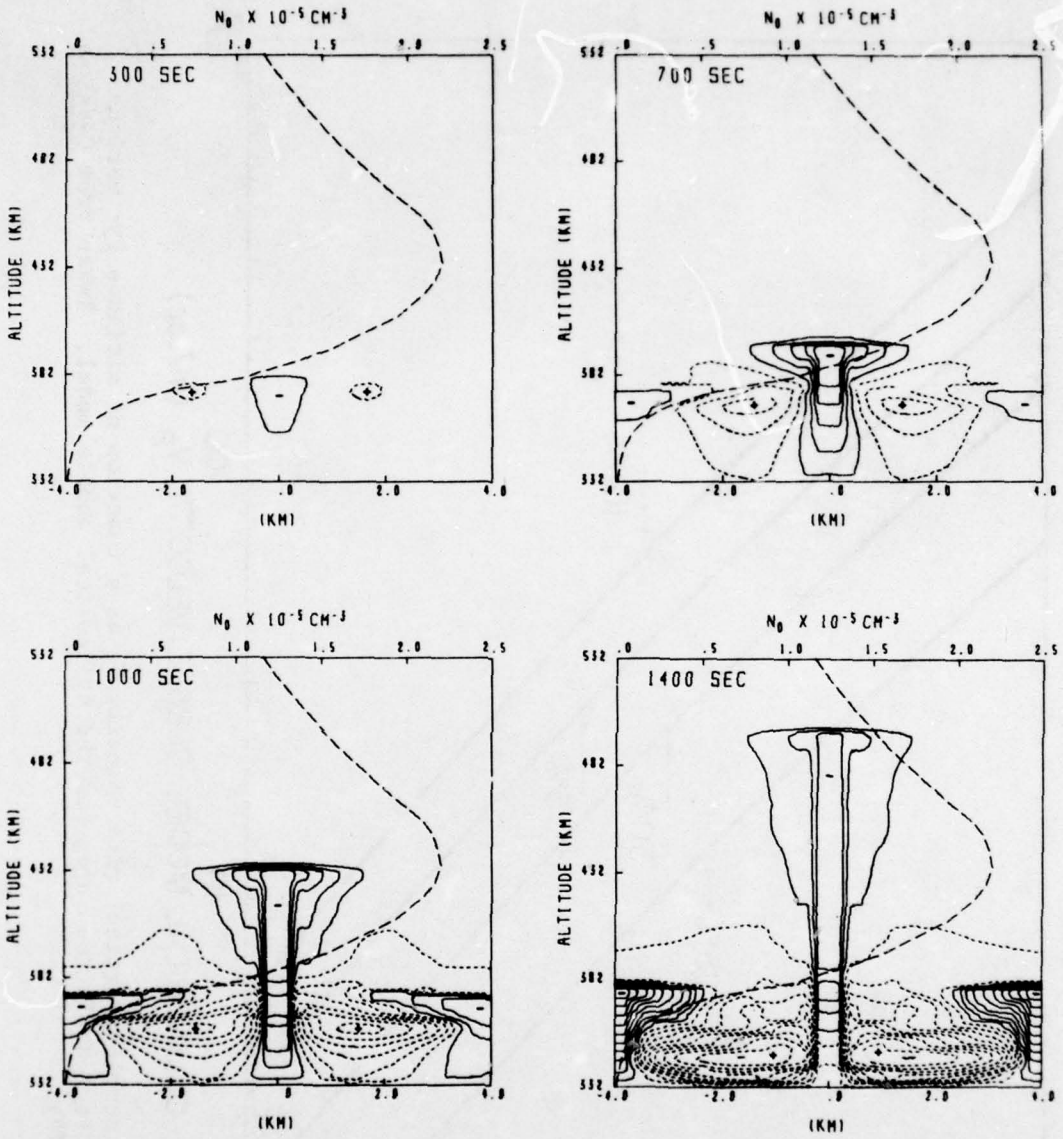

Fig. 5 - Contour plots of constant n_1/n_o for the F peak at 434km simulation at t = 300, 700, 1000, and 1400 sec. All other nomenclature is same as Fig. 3. Taken from Ossakow et al. (1978)

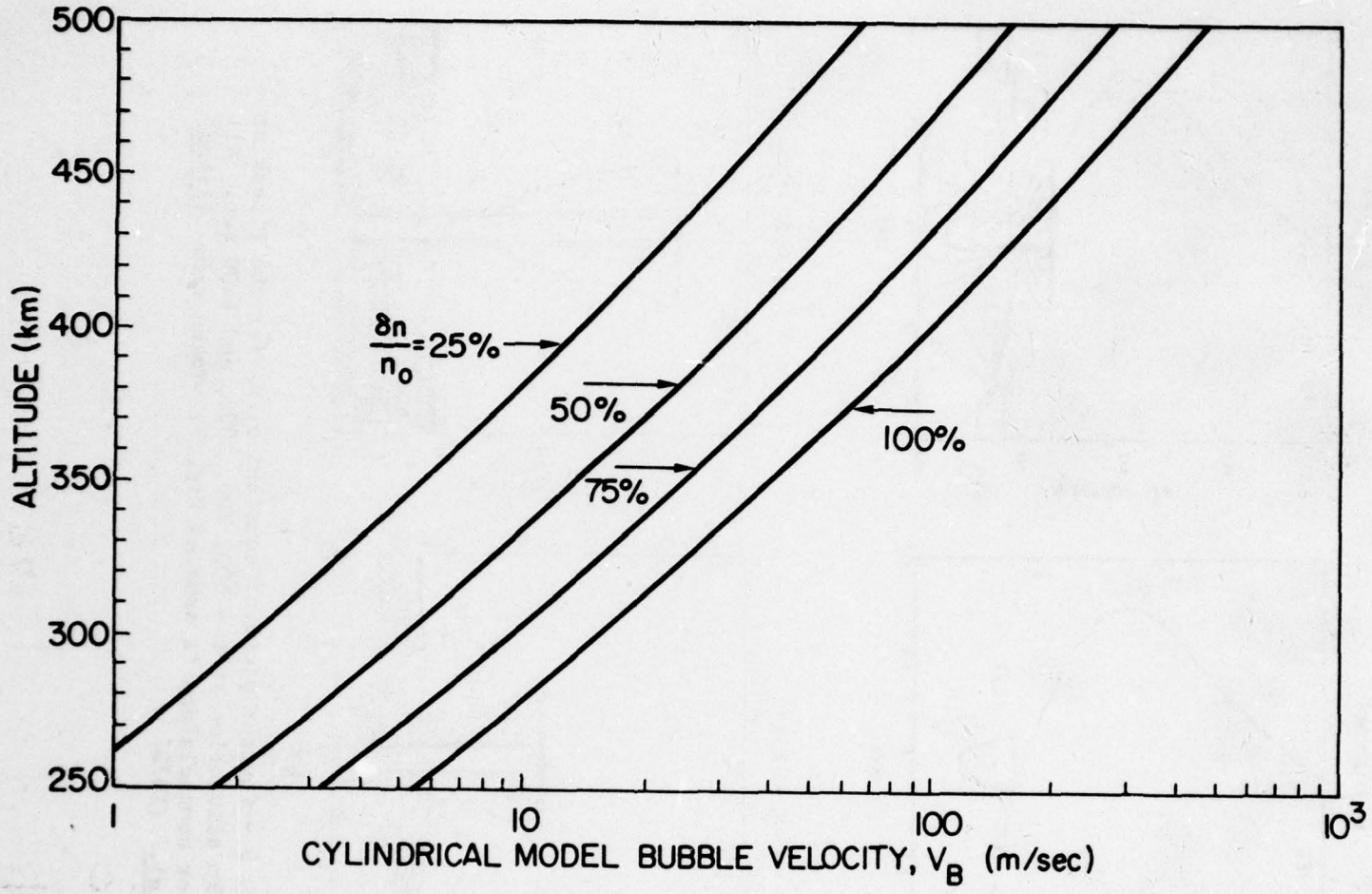

Fig. 6 - Depletion (bubble) vertical rise velocity V_B as a function of altitude for various values of the percentage depletion $\delta n/n_o$ for the cylindrical bubble model. Taken from Ossakow and Chaturvedi (1978)

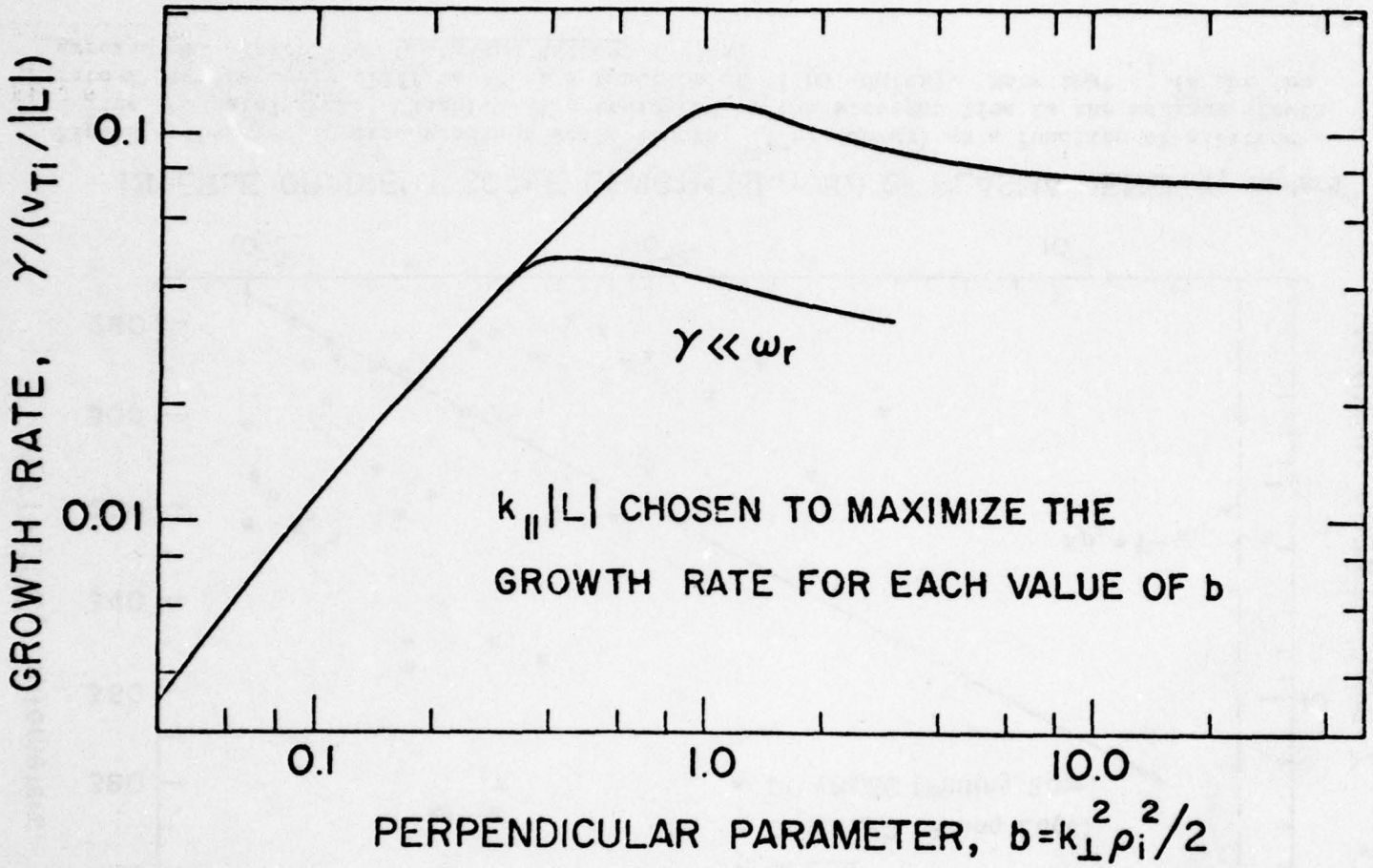

Fig. 7 - Growth rates as a function of b for the low frequency collisionless drift waves (ρ_i is the ion gyroradius). The curve $\gamma << \omega_r$ is obtained from a small growth rate approximation expression. Taken from Costa and Kelley (1978b)

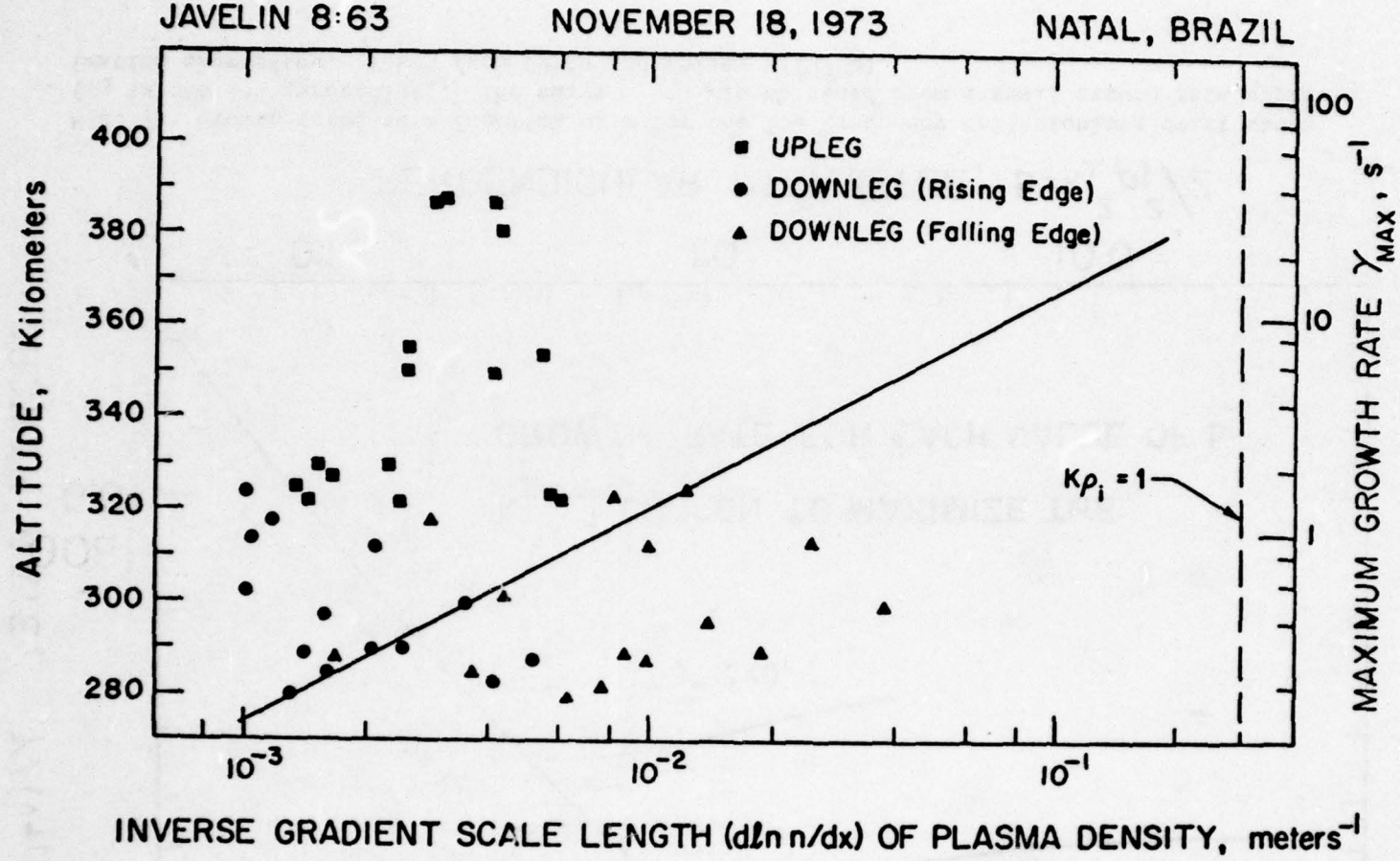

Fig. 8 - Observed inverse gradient scale lengths (1/n) (dn/dx) as a function of altitude during the Natal rocket flight. Also indicated by the straight line is the maximum growth rate of low frequency drift waves as a function of (1/n) (dn/dx). Note that ρ_i is the ion gyroradius. Taken from Costa and Kelley (1978a)

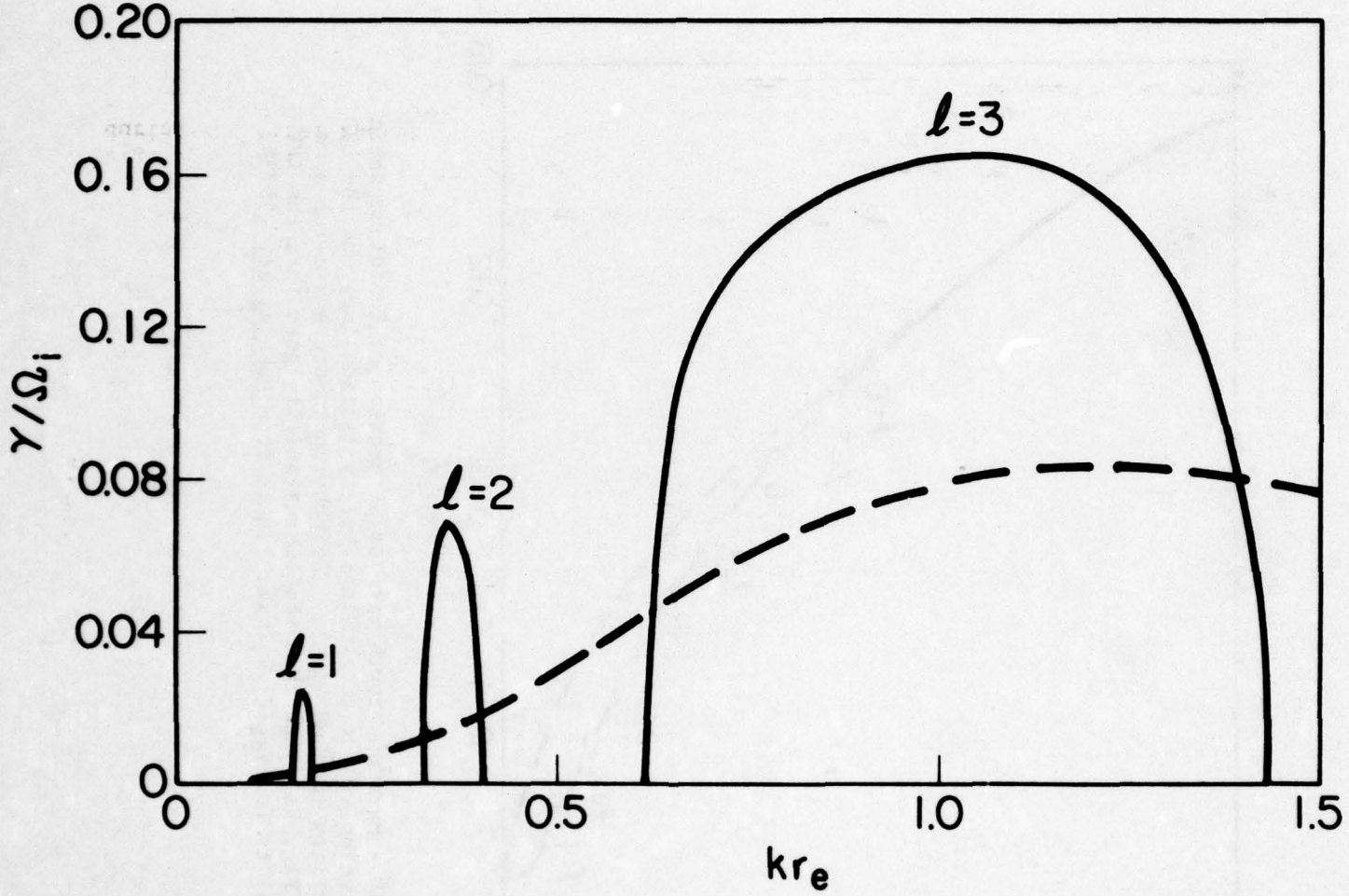

Fig. 9 - Growth rate as a function of perpendicular wavenumber for the DC instability (solid line) and LHD instability (dashed line) for an 0^+ plasma with $T_e = T_i$, $\omega_{pe}/\Omega_e = 10$ (where ω_{pe} is the electron plasma frequency), and $V_{di}/V_i = 0.037$. Growth also occurs for $kr_e > 1.5$, but has not been plotted. Taken from Huba et al. (1978)

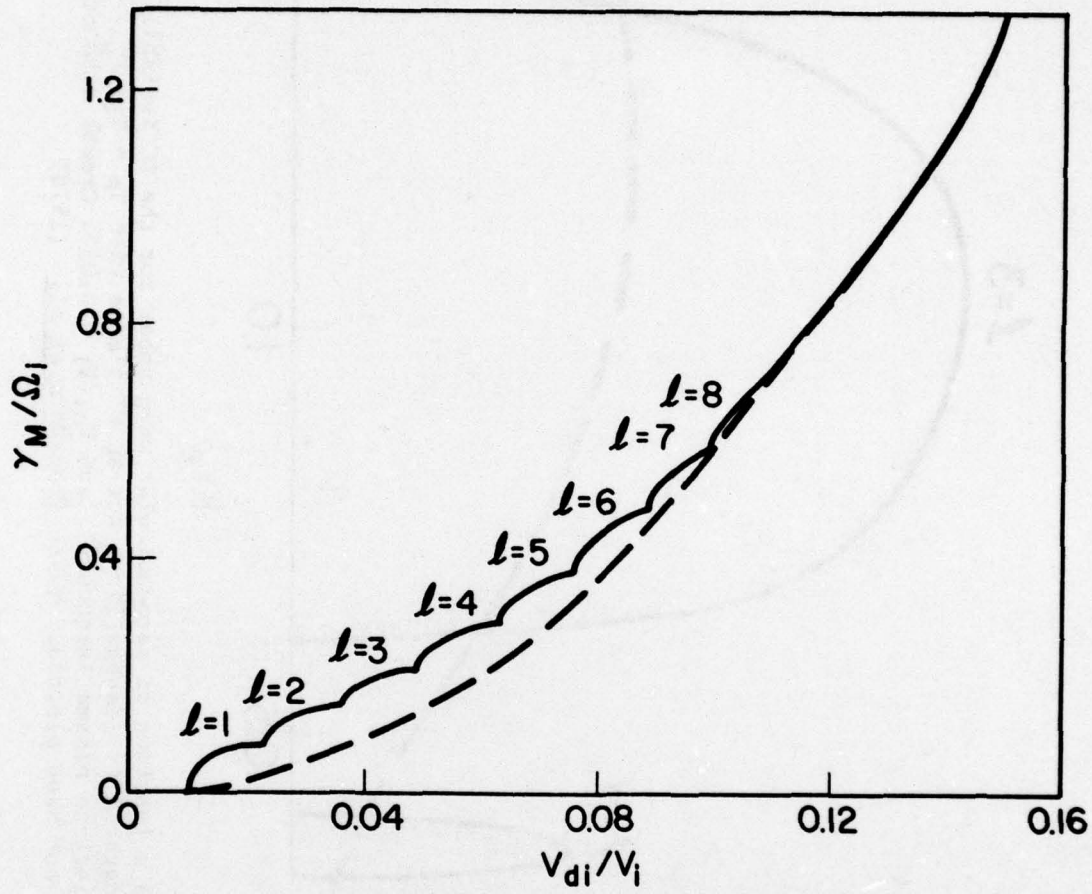

Fig. 10 - Maximum growth rate as a function of ion diamagnetic drift velocity for the DC instability (solid line) and the LHD instability (dashed line). The other parameters are the same as in Fig. 9. Note that the DC instability goes into the LHD instbility for $V_{di}/V_i \geq 0.11$. Taken from Huba et al. (1978)

DISTRIBUTION LIST

DEPARTMENT OF DEFENSE

ASSISTANT SECRETARY OF DEFENSE
COMM, CMD, CONT & INTELL
WASHINGTON, D.C. 20301
01CY ATTN J. BABCOCK
01CY ATTN M. EPSTEIN

ASSISTANT TO THE SECRETARY OF DEFENSE
ATOMIC ENERGY
WASHINGTON, D.C. 20301
01CY ATTN EXECUTIVE ASSISTANT

DIRECTOR
COMMAND CONTROL TECHNICAL CENTER
PENTAGON RM BE 685
WASHINGTON, D.C. 20301
01CY ATTN C-650
01CY ATTN C-312 R. MASON

DIRECTOR
DEFENSE ADVANCED RSCH PROJ AGENCY
ARCHITECT BUILDING
1400 WILSON BLVD.
ARLINGTON, VA. 22209
01CY ATTN NUCLEAR MONITORING RESEARCH
01CY ATTN STRATEGIC TECH OFFICE

DEFENSE COMMUNICATION ENGINEER CENTER
1860 WIEHLE AVENUE
RESTON, VA. 22090
01CY ATTN CODE R820
01CY ATTN CODE R410 JAMES W. MCLEAN
01CY ATTN CODE R720 J. WORTHINGTON

DEFENSE DOCUMENTATION CENTER
CAMERON STATION
ALEXANDRIA, VA. 22314
(12 COPIES IF OPEN PUBLICATION, OTHERWISE 2 COPIES)
12CY ATTN TC

DIRECTOR
DEFENSE INTELLIGENCE AGENCY
WASHINGTON, D.C. 20301
01CY ATTN DT-1B
01CY ATTN DB-4C E. O'FARRELL
01CY ATTN DIAAP A. WISE
01CY ATTN DIAST-5
01CY ATTN DT-1B2 R. MORTON
01CY ATTN HQ-TR J. STEWART
01CY ATTN W. WITTIG DC-7D

DIRECTOR
DEFENSE NUCLEAR AGENCY
WASHINGTON, D.C. 20305
01CY ATTN STVL
04CY ATTN TITL
01CY ATTN DDST
03CY ATTN RAAE

COMMANDER
FIELD COMMAND
DEFENSE NUCLEAR AGENCY
KIRTLAND AFB, NM 87115
01CY ATTN FCPR

DIRECTOR
INTERSERVICE NUCLEAR WEAPONS SCHOOL
KIRTLAND AFB, NM 87115
01CY ATTN DOCUMENT CONTROL

JOINT CHIEFS OF STAFF
WASHINGTON, D.C. 20301
01CY ATTN J-3 WWMCCS EVALUATION OFFICE

DIRECTOR
JOINT STRAT TGT PLANNING STAFF
OFFUTT AFB
OMAHA, NB 68113
01CY ATTN JLTW-2
01CY ATTN JPST G. GOETZ

CHIEF
LIVERMORE DIVISION FLD COMMAND DNA
DEPARTMENT OF DEFENSE
LAWRENCE LIVERMORE LABORATORY
P. O. BOX 808
LIVERMORE, CA 94550
01CY ATTN FCPRL

DIRECTOR
NATIONAL SECURITY AGENCY
DEPARTMENT OF DEFENSE
FT. GEORGE G. MEADE, MD 20755
01CY ATTN JOHN SKILLMAN R52
01CY ATTN FRANK LEONARD
01CY ATTN W14 PAT CLARK
01CY ATTN OLIVER M. BARTLETT W32
01CY ATTN R5

COMMANDANT
NATO SCHOOL (SHAPE)
APO NEW YORK 09172
01CY ATTN U.S. DOCUMENTS OFFICER

UNDER SECY OF DEF FOR RSCH & ENGRG
DEPARTMENT OF DEFENSE
WASHINGTON, D.C. 20301
01CY ATTN STRATEGIC & SPACE SYSTEMS (OS)

WWMCCS SYSTEM ENGINEERING ORG
WASHINGTON, D.C. 20305
01CY ATTN R. CRAWFORD

COMMANDER/DIRECTOR
ATMOSPHERIC SCIENCES LABORATORY
U.S. ARMY ELECTRONICS COMMAND
WHITE SANDS MISSILE RANGE, NM 88002
01CY ATTN DELAS-EO F. NILES

DIRECTOR
BMD ADVANCED TECH CTR
HUNTSVILLE OFFICE
P. O. BOX 1500
HUNTSVILLE, AL 35807
01CY ATTN ATC-T MELVIN T. CAPPS
01CY ATTN ATC-O W. DAVIES
01CY ATTN ATC-R DON RUSS

PROGRAM MANAGER
BMD PROGRAM OFFICE
5001 EISENHOWER AVENUE
ALEXANDRIA, VA 22333
01CY ATTN DACS-BMT J. SHEA

CHIEF C-E SERVICES DIVISION
U.S. ARMY COMMUNICATIONS CMD
PENTAGON RM 1B269
WASHINGTON, D.C. 20310
01CY ATTN C-E-SERVICES DIVISION

COMMANDER
FRADCOM TECHNICAL SUPPORT ACTIVITY
DEPARTMENT OF THE ARMY
FORT MONMOUTH, N.J. 07703
01CY ATTN DRSEL-NL-RD H. BENNET
01CY ATTN DRSEL-PL-ENV H. BOMKE
01CY ATTN J. E. QUIGLEY

COMMANDER
HARRY DIAMOND LABORATORIES
DEPARTMENT OF THE ARMY
2800 POWDER MILL ROAD
ADELPHI, MD 20783
(CNWDI-INNER ENVELOPE: ATTN: DELHD-RBH)
01CY ATTN DELHD-TI M. WEINER
01CY ATTN DELHD-RB R. WILLIAMS
01CY ATTN DELHD-NP F. WIMENITZ
01CY ATTN DELHD-NP C. MOAZED

COMMANDER
U.S. ARMY COMM-ELEC ENGRG INSTAL AGY
FT. HUACHUCA, AZ 85613
01CY ATTN CCC-EMEO GEORGE LANE

COMMANDER
U.S. ARMY FOREIGN SCIENCE & TECH CTR
220 7TH STREET, NE
CHARLOTTESVILLE, VA 22901
01CY ATTN DRXST-SD
01CY ATTN R. JONES

COMMANDER
U.S. ARMY MATERIEL DEV & READINESS CMD
5001 EISENHOWER AVENUE
ALEXANDRIA, VA 22333
01CY ATTN DRCLDC J. A. BENDER

COMMANDER
U.S. ARMY NUCLEAR AND CHEMICAL AGENCY
7500 BACKLICK ROAD
BLDG 2073
SPRINGFIELD, VA 22150
01CY ATTN LIBRARY

DIRECTOR
U.S. ARMY BALLISTIC RESEARCH LABS
ABERDEEN PROVING GROUND, MD 21005
01CY ATTN TECH LIB EDWARD BAICY

COMMANDER
U.S. ARMY SATCOM AGENCY
FT. MONMOUTH, NJ 07703
01CY ATTN DOCUMENT CONTROL

COMMANDER
U.S. ARMY MISSILE INTELLIGENCE AGENCY
REDSTONE ARSENAL, AL 35809
01CY ATTN JIM GAMBLE

DIRECTOR
U.S. ARMY TRADOC SYSTEMS ANALYSIS ACTIVITY
WHITE SANDS MISSILE RANGE, NM 88002
01CY ATTN ATAA-SA
01CY ATTN TCC/F. PAYAN JR.
01CY ATTN ATAA-TAC LTC J. MESSE

COMMANDER
NAVAL ELECTRONIC SYSTEMS COMMAND
WASHINGTON, D.C. 20360
01CY ATTN NAVALEX 034 T. HUGHES
01CY ATTN PME 117
01CY ATTN PME 117-T
01CY ATTN CODE 5011

COMMANDING OFFICER
NAVAL INTELLIGENCE SUPPORT CTR
4301 SUITLAND ROAD, BLDG. 5
WASHINGTON, D.C. 20390
01CY ATTN MR. DUBBIN STIC 12
01CY ATTN NISC-50
01CY ATTN CODE 5404 J. GALET

COMMANDER
NAVAL SURFACE WEAPONS CENTER
DAHLGREN LABORATORY
DAHLGREN, VA 22448
01CY ATTN CODE DF-14 R. BUTLER

COMMANDING OFFICER
NAVY SPACE SYSTEMS ACTIVITY
P.O. BOX 92960
WORLDWAY POSTAL CENTER
LOS ANGELES, CA. 90009
01CY ATTN CODE 52

OFFICE OF NAVAL RESEARCH
ARLINGTON, VA 22217
01CY ATTN CODE 465
01CY ATTN CODE 461
01CY ATTN CODE 402
01CY ATTN CODE 420
01CY ATTN CODE 421

COMMANDER
AEROSPACE DEFENSE COMMAND/DC
DEPARTMENT OF THE AIR FORCE
ENT AFB, CO 80912
01CY ATTN DC MR. LONG

COMMANDER
AEROSPACE DEFENSE COMMAND/XPD
DEPARTMENT OF THE AIR FORCE
ENT AFB, CO 80912
01CY ATTN XPDQQ
01CY ATTN XP

AIR FORCE GEOPHYSICS LABORATORY
HANSCOM AFB, MA 01731
01CY ATTN OPR HAROLD GARDNER
01CY ATTN OPR-1 JAMES C. ULWICK
01CY ATTN LKB KENNETH S. W. CHAMPION
01CY ATTN OPR ALVA T. STAIR
01CY ATTN PHP JULES AARONS
01CY ATTN PHD JURGEN BUCHAU
01CY ATTN PHD JOHN P. MULLEN

AF WEAPONS LABORATORY
KIRTLAND AFB, NM 87117
01CY ATTN SUL
01CY ATTN CA ARTHUR H. GUENTHER
01CY ATTN DYC CAPT J. BARRY
01CY ATTN DYC JOHN M. KAMM
01CY ATTN DYT CAPT MARK A. FRY
01CY ATTN DES MAJ GARY GANONG
01CY ATTN DYC J. JANNI

AFTAC
PATRICK AFB, FL 32925
01CY ATTN TF/MAJ WILEY
01CY ATTN TN

AIR FORCE AVIONICS LABORATORY
WRIGHT-PATTERSON AFB, OH 45433
01CY ATTN AAD WADE HUNT
01CY ATTN AAD ALLEN JOHNSON

DEPUTY CHIEF OF STAFF
RESEARCH, DEVELOPMENT, & ACQ
DEPARTMENT OF THE AIR FORCE
WASHINGTON, D.C. 20330
01CY ATTN AFRDQ

HEADQUARTERS
ELECTRONIC SYSTEMS DIVISION/XR
DEPARTMENT OF THE AIR FORCE
HANSCOM AFB, MA 01731
01CY ATTN XR J. DEAS

HEADQUARTERS
ELECTRONIC SYSTEMS DIVISION/YSEA
DEPARTMENT OF THE AIR FORCE
HANSCOM AFB, MA 01731
01CY ATTN YSEA

COMMANDER
NAVAL OCEAN SYSTEMS CENTER
SAN DIEGO, CA 92152
03CY ATTN CODE 532 W. MOLER
01CY ATTN CODE 0230 C. BAGGETT
01CY ATTN CODE 81 R. EASTMAN

DIRECTOR
NAVAL RESEARCH LABORATORY
WASHINGTON, D.C. 20375
01CY ATTN CODE 6700 TIMOTHY P. COFFEY
(25 CYS IF UNCLASS, 1 CY IF CLASS)
01CY ATTN CODE 6701 JACK D. BROWN
01CY ATTN CODE 6780 BRANCH HEAD (150 CYS
IF UNCLASS, 1 CY IF CLASS)
01CY ATTN CODE 7500 HQ COMM DIR BRUCE WALD
01CY ATTN CODE 7550 J. DAVIS
01CY ATTN CODE 7580
01CY ATTN CODE 7551
01CY ATTN CODE 7555
01CY ATTN CODE 6730 E. MCLEAN
01CY ATTN CODE 7127 C. JOHNSON

COMMANDER
NAVAL SEA SYSTEMS COMMAND
WASHINGTON, D.C. 20362
01CY ATTN CAPT R. PITKIN

COMMANDER
NAVAL SPACE SURVEILLANCE SYSTEM
DAHLGREN, VA 22448
01CY ATTN CAPT J. H. BURTON

OFFICER-IN-CHARGE
NAVAL SURFACE WEAPONS CENTER
WHITE OAK, SILVER SPRING, MD 20910
01CY ATTN CODE F31

DIRECTOR
STRATEGIC SYSTEMS PROJECT OFFICE
DEPARTMENT OF THE NAVY
WASHINGTON, D.C. 20376
01CY ATTN NSP-2141
01CY ATTN NSSP-2722 FRED WIMBERLY

NAVAL SPACE SYSTEM ACTIVITY
P. O. BOX 92960
WORLDWAY POSTAL CENTER
LOS ANGELES, CALIF. 90009
01CY ATTN A. B. HAZZARD

HEADQUARTERS
ELECTRONIC SYSTEMS DIVISION/DC
DEPARTMENT OF THE AIR FORCE
HANSCOM AFB, MA 01731
01CY ATTN DOKC MAJ J. C. CLARK

COMMANDER
FOREIGN TECHNOLOGY DIVISION, AFSC
WRIGHT-PATTERSON AFB, OH 45433
01CY ATTN NICD LIBRARY
01CY ATTN ETDP B. BALLARD

COMMANDER
ROME AIR DEVELOPMENT CENTER, AFSC
GRIFFISS AFB, NY 13441
01CY ATTN DOC LIBRARY/TSLD
01CY ATTN OCSE V. COYNE

SAMSO/SZ
POST OFFICE BOX 92960
WORLDWAY POSTAL CENTER
LOS ANGELES, CA 90009
(SPACE DEFENSE SYSTEMS)
01CY ATTN SZJ

STRATEGIC AIR COMMAND/XPFS
OFFUTT AFB, NB 68113
01CY ATTN XPFS MAJ B. STEPHAN
01CY ATTN ADWATE MAJ BRUCE BAUER
01CY ATTN NRT
01CY ATTN DOK CHIEF SCIENTIST

SAMSO/YA
P. O. BOX 92960
WORLDWAY POSTAL CENTER
LOS ANGELES, CA 90009
01CY ATTN YAT CAPT L. BLACKWELDER

SAMSO/SK
P. O. BOX 92960
WORLDWAY POSTAL CENTER
LOS ANGELES, CA 90009
01CY ATTN SKA (SPACE COMM SYSTEMS) M. CLAVIN

SAMSO/MN
NORTON AFB, CA 92409
(MINUTEMAN)
01CY ATTN MNNL LTC KENNEDY

COMMANDER
ROME AIR DEVELOPMENT CENTER, AFSC
HANSCOM AFB, MA 01731
01CY ATTN EEP A. LORENTZEN

DEPARTMENT OF ENERGY

DEPARTMENT OF ENERGY
ALBUQUERQUE OPERATIONS OFFICE
P. O. BOX 5400
ALBUQUERQUE, NM 87115
01CY ATTN DOC CON FOR D. SHERWOOD

DEPARTMENT OF ENERGY
LIBRARY ROOM G-042
WASHINGTON, D.C. 20545
01CY ATTN DOC CON FOR A. LABOWITZ

EG&G, INC.
LOS ALAMOS DIVISION
P. O. BOX 809
LOS ALAMOS, NM 85544
01CY ATTN DOC CON FOR J. BREEDLOVE

UNIVERSITY OF CALIFORNIA
LAWRENCE LIVERMORE LABORATORY
P. O. BOX 808
LIVERMORE, CA 94550
01CY ATTN DOC CON FOR TECH INFO DEPT
01CY ATTN DOC CON FOR L-389 R. OTT
01CY ATTN DOC CON FOR L-31 R. HAGER
01CY ATTN DOC CON FOR L-46 F. SEWARD

LOS ALAMOS SCIENTIFIC LABORATORY
P. O. BOX 1663
LOS ALAMOS, NM 87545
01CY ATTN DOC CON FOR J. WOLCOTT
01CY ATTN DOC CON FOR R. F. TASCHEK
01CY ATTN DOC CON FOR E. JONES
01CY ATTN DOC CON FOR J. MALIK
01CY ATTN DOC CON FOR R. JEFFRIES
01CY ATTN DOC CON FOR J. ZINN
01CY ATTN DOC CON FOR P. KEATON
01CY ATTN DOC CON FOR D. WESTERVELT

SANDIA LABORATORIES
P. O. BOX 5800
ALBUQUERQUE, NM 87115
01CY ATTN DOC CON FOR J. MARTIN
01CY ATTN DOC CON FOR W. BROWN
01CY ATTN DOC CON FOR A. THORNBROUGH
01CY ATTN DOC CON FOR T. WRIGHT
01CY ATTN DOC CON FOR D. DAHLGREN
01CY ATTN DOC CON FOR 3141
01CY ATTN DOC CON FOR SPACE PROJECT DIV

SANDIA LABORATORIES
LIVERMORE LABORATORY
P. O. BOX 969
LIVERMORE, CA 94550
01CY ATTN DOC CON FOR B. MURPHEY
01CY ATTN DOC CON FOR T. COOK

OFFICE OF MILITARY APPLICATION
DEPARTMENT OF ENERGY
WASHINGTON, D.C. 20545
01CY ATTN DOC CON FOR D. GALE

OTHER GOVERNMENT

CENTRAL INTELLIGENCE AGENCY
ATTN RD/SI, RM 5G48, HQ BLDG
WASHINGTON, D.C. 20505
01CY ATTN OSI/PSID RM 5F 19

DEPARTMENT OF COMMERCE
NATIONAL BUREAU OF STANDARDS
WASHINGTON, D.C. 20234
(ALL CORRES: ATTN SEC OFFICER FOR)
01CY ATTN R. MOORE

DEPARTMENT OF TRANSPORTATION
OFFICE OF THE SECRETARY
TAD-44.1, ROOM 10402-B
400 7TH STREET, S.W.
WASHINGTON, D.C. 20590
01CY ATTN R. LEWIS
01CY ATTN R. DOHERTY

INSTITUTE FOR TELECOM SCIENCES
NATIONAL TELECOMMUNICATIONS & INFO ADMIN
BOULDER, CO 80303
01CY ATTN A. JEAN (UNCLASS ONLY)
01CY ATTN W. UTLAUT
01CY ATTN D. CROMBIE
01CY ATTN L. BERRY

NATIONAL OCEANIC & ATMOSPHERIC ADMIN
ENVIRONMENTAL RESEARCH LABORATORIES
DEPARTMENT OF COMMERCE
BOULDER, CO 80302
01CY ATTN R. GRUBB
01CY ATTN AERONOMY LAB G. REID

DEPARTMENT OF DEFENSE CONTRACTORS

AEROSPACE CORPORATION
P. O. BOX 92957
LOS ANGELES, CA 90009
01CY ATTN I. GARFUNKEL
01CY ATTN T. SALMI
01CY ATTN V. JOSEPHSON
01CY ATTN S. BOWER
01CY ATTN N. STOCKWELL
01CY ATTN D. OLSEN
01CY ATTN J. CARTER
01CY ATTN F. MORSE
01CY ATTN SMFA FOR PWW

ANALYTICAL SYSTEMS ENGINEERING CORP
5 OLD CONCORD ROAD
BURLINGTON, MA 01803
01CY ATTN RADIO SCIENCES

BERKELEY RESEARCH ASSOCIATES, INC.
P. O. BOX 983
BERKELEY, CA 94701
01CY ATTN J. WORKMAN

BOEING COMPANY, THE
P. O. BOX 3707
SEATTLE, WA 98124
01CY ATTN G. KEISTER
01CY ATTN D. MURRAY
01CY ATTN G. HALL
01CY ATTN J. KENNEY

CALIFORNIA AT SAN DIEGO, UNIV OF
IPAPS, B-019
LA JOLLA, CA 92093
01CY ATTN HENRY G. BOOKER

BROWN ENGINEERING COMPANY, INC.
CUMMINGS RESEARCH PARK
HUNTSVILLE, AL 35807
01CY ATTN ROMEO A. DELIBERIS

CHARLES STARK DRAPER LABORATORY, INC.
555 TECHNOLOGY SQUARE
CAMBRIDGE, MA 02139
01CY ATTN D. B. COX
01CY ATTN J. P. GILMORE

COMPUTER SCIENCES CORPORATION
6565 ARLINGTON BLVD
FALLS CHURCH, VA 22046
01CY ATTN H. BLANK
01CY ATTN JOHN SPOOR
01CY ATTN C. NAIL

COMSAT LABORATORIES
LINTHICUM ROAD
CLARKSBURG, MD 20734
01CY ATTN G. HYDE

CORNELL UNIVERSITY
DEPARTMENT OF ELECTRICAL ENGINEERING
ITHACA, NY 14850
01CY ATTN D. T. FARLEY JR

ELECTROSPACE SYSTEMS, INC.
BOX 1359
RICHARDSON, TX 75080
01CY ATTN H. LOGSTON
01CY ATTN SECURITY (PAUL PHILLIPS)

ESL INC.
495 JAVA DRIVE
SUNNYVALE, CA 94086
01CY ATTN J. ROBERTS
01CY ATTN JAMES MARSHALL
01CY ATTN C. W. PRETTIE

FORD AEROSPACE & COMMUNICATIONS CORP
3939 FABIAN WAY
PALO ALTO, CA 94303
01CY ATTN J. T. MATTINGLEY

GENERAL ELECTRIC COMPANY
SPACE DIVISION
VALLEY FORGE SPACE CENTER
GODDARD BLVD KING OF PRUSSIA
P. O. BOX 8555
PHILADELPHIA, PA 19101
01CY ATTN M. H. BORTNER SPACE SCI LAB

GENERAL ELECTRIC COMPANY
P. O. BOX 1122
SYRACUSE, NY 13201
01CY ATTN F. REIBERT

GENERAL ELECTRIC COMPANY
TEMPO-CENTER FOR ADVANCED STUDIES
816 STATE STREET (P.O. DRAWER QQ)
SANTA BARBARA, CA 93102
01CY ATTN DASIAC
01CY ATTN DON CHANDLER
01CY ATTN TOM BARRETT
01CY ATTN TIM STEPHANS
01CY ATTN WARREN S. KNAPP
01CY ATTN WILLIAM MCNAMARA
01CY ATTN B. GAMBILL
01CY ATTN MACK STANTON

GENERAL ELECTRIC TECH SERVICES CO., INC.
HMES
COURT STREET
SYRACUSE, NY 13201
01CY ATTN G. MILLMAN

GENERAL RESEARCH CORPORATION
SANTA BARBARA DIVISION
P. O. BOX 6770
SANTA BARBARA, CA 93111
01CY ATTN JOHN ISE JR
01CY ATTN JOEL GARBARINO

GEOPHYSICAL INSTITUTE
UNIVERSITY OF ALASKA
FAIRBANKS, AK 99701
(ALL CLASS ATTN: SECURITY OFFICER)
01CY ATTN T. N. DAVIS (UNCL ONLY)
01CY ATTN NEAL BROWN (UNCL ONLY)
01CY ATTN TECHNICAL LIBRARY

GTE SYLVANIA, INC.
ELECTRONICS SYSTEMS GRP-EASTERN DIV
77 A STREET
NEEDHAM, MA 02194
01CY ATTN MARSHAL CROSS

ILLINOIS, UNIVERSITY OF
DEPARTMENT OF ELECTRICAL ENGINEERING
URBANA, IL 61803
01CY ATTN K. YEH

ILLINOIS, UNIVERSITY OF
107 COBLE HALL
801 S. WRIGHT STREET
URBANA, IL 60680
(ALL CORRES ATTN SECURITY SUPERVISOR FOR)
01CY ATTN K. YEH

INSTITUTE FOR DEFENSE ANALYSES
400 ARMY-NAVY DRIVE
ARLINGTON, VA 22202
01CY ATTN J. M. AEIN
01CY ATTN ERNEST BAUER
01CY ATTN HANS WOLFHARD
01CY ATTN JOEL BENGSTON

HSS, INC.
2 ALFRED CIRCLE
BEDFORD, MA 01730
01CY ATTN DONALD HANSEN

INTL TEL & TELEGRAPH CORPORATION
500 WASHINGTON AVENUE
NUTLEY, NJ 07110
01CY ATTN TECHNICAL LIBRARY

JAYCOR
1401 CAMINO DEL MAR
DEL MAR, CA 92014
01CY ATTN S. R. GOLDMAN

JOHNS HOPKINS UNIVERSITY
APPLIED PHYSICS LABORATORY
JOHNS HOPKINS ROAD
LAUREL, MD 20810
01CY ATTN DOCUMENT LIBRARIAN
01CY ATTN THOMAS POTEMRA
01CY ATTN JOHN DASSOULAS

LOCKHEED MISSILES & SPACE CO INC
P. O. BOX 504
SUNNYVALE, CA 94088
01CY ATTN DEPT 60-12
01CY ATTN D. R. CHURCHILL

LOCKHEED MISSILES AND SPACE CO INC
3251 HANOVER STREET
PALO ALTO, CA 94304
01CY ATTN MARTIN WALT DEPT 52-10
01CY ATTN RICHARD G. JOHNSON DEPT 52-12
01CY ATTN W. L. IMHOF DEPT 52-12

KAMAN SCIENCES CORP
P. O. BOX 7463
COLORADO SPRINGS, CO 80933
01CY ATTN T. MEAGHER

LINKABIT CORP
10453 ROSELLE
SAN DIEGO, CA 92121
01CY ATTN IRWIN JACOBS

LOWELL RSCH FOUNDATION, UNIVERSITY OF
450 AIKEN STREET
LOWELL, MA 01854
01CY ATTN K. BIBL

M.I.T. LINCOLN LABORATORY
P. O. BOX 73
LEXINGTON, MA 02173
01CY ATTN DAVID M. TOWLE
01CY ATTN P. WALDRON
01CY ATTN L. LOUGHLIN
01CY ATTN D. CLARK

MARTIN MARIETTA CORP
ORLANDO DIVISION
P. O. BOX 5837
ORLANDO, FL 32805
01CY ATTN R. HEFFNER

MCDONNELL DOUGLAS CORPORATION
5301 BOLSA AVENUE
HUNTINGTON BEACH, CA 92647
01CY ATTN N. HARRIS
01CY ATTN J. MOULE
01CY ATTN GEORGE MROZ
01CY ATTN W. OLSON
01CY ATTN R. W. HALPRIN
01CY ATTN TECHNICAL LIBRARY SERVICES

MISSION RESEARCH CORPORATION
735 STATE STREET
SANTA BARBARA, CA 93101
01CY ATTN P. FISCHER
01CY ATTN W. F. CREVIER
01CY ATTN STEVEN L. GUTSCHE
01CY ATTN D. SAPPENFIELD
01CY ATTN R. BOGUSCH
01CY ATTN R. HENDRICK
01CY ATTN RALPH KILB
01CY ATTN DAVE SOWLE
01CY ATTN F. FAJEN
01CY ATTN M. SCHEIBE
01CY ATTN CONRAD L. LONGMIRE
01CY ATTN WARREN A. SCHLUETER

MITRE CORPORATION, THE
P. O. BOX 208
BEDFORD, MA 01730
01CY ATTN JOHN MORGANSTERN
01CY ATTN G. HARDING
01CY ATTN C. E. CALLAHAN

MITRE CORP
WESTGATE RESEARCH PARK
1820 DOLLY MADISON BLVD
MCLEAN, VA 22101
01CY ATTN W. HALL
01CY ATTN W. FOSTER

PACIFIC-SIERRA RESEARCH CORP
1456 CLOVERFIELD BLVD.
SANTA MONICA, CA 90404
01CY ATTN E. C. FIELD JR

PENNSYLVANIA STATE UNIVERSITY
IONOSPHERE RESEARCH LAB
318 ELECTRICAL ENGINEERING EAST
UNIVERSITY PARK, PA 16802
(NO CLASSIFIED TO THIS ADDRESS)
01CY ATTN IONOSPHERIC RESEARCH LAB

PHOTOMETRICS, INC.
442 MARRETT ROAD
LEXINGTON, MA 02173
01CY ATTN IRVING L. KOFSKY

PHYSICAL DYNAMICS INC.
P. O. BOX 3027
BELLEVUE, WA 98009
01CY ATTN E. J. FREMOUW

PHYSICAL DYNAMICS INC.
P. O. BOX 1069
BERKELEY, CA 94701
01CY ATTN A. THOMPSON

R & D ASSOCIATES
P. O. BOX 9695
MARINA DEL REY, CA 90291
01CY ATTN FORREST GILMORE
01CY ATTN BRYAN GABBARD
01CY ATTN WILLIAM B. WRIGHT JR
01CY ATTN ROBERT F. LELEVIER
01CY ATTN WILLIAM J. KARZAS
01CY ATTN H. ORY
01CY ATTN C. MACDONALD
01CY ATTN R. TURCO

RAND CORPORATION, THE
1700 MAIN STREET
SANTA MONICA, CA 90406
01CY ATTN CULLEN CRAIN
01CY ATTN ED BEDROZIAN

RIVERSIDE RESEARCH INSTITUTE
80 WEST END AVENUE
NEW YORK, NY 10023
01CY ATTN VINCE TRAPANI

SCIENCE APPLICATIONS, INC.
P. O. BOX 2351
LA JOLLA, CA 92038
01CY ATTN LEWIS M. LINSON
01CY ATTN DANIEL A. HAMLIN
01CY ATTN D. SACHS
01CY ATTN E. A. STRAKER
01CY ATTN CURTIS A. SMITH
01CY ATTN JACK MCDOUGALL

RAYTHEON CO.
528 BOSTON POST ROAD
SUDBURY, MA 01776
01CY ATTN BARBARA ADAMS

SCIENCE APPLICATIONS, INC.
HUNTSVILLE DIVISION
2109 W. CLINTON AVENUE
SUITE 700
HUNTSVILLE, AL 35805
01CY ATTN DALE H. DIVIS

SCIENCE APPLICATIONS, INCORPORATED
8400 WESTPARK DRIVE
MCLEAN, VA 22101
01CY ATTN J. COCKAYNE

SCIENCE APPLICATIONS, INC.
80 MISSION DRIVE
PLEASANTON, CA 94566
01CY ATTN SZ

SRI INTERNATIONAL
333 RAVENSWOOD AVENUE
MENLO PARK, CA 94025
01CY ATTN DONALD NEILSON
01CY ATTN ALAN BURNS
01CY ATTN G. SMITH
01CY ATTN L. L. COBB
01CY ATTN DAVID A. JOHNSON
01CY ATTN WALTER G. CHESNUT
01CY ATTN CHARLES L. RINO
01CY ATTN WALTER JAYE
01CY ATTN M. BARON
01CY ATTN RAY L. LEADABRAND
01CY ATTN G. CARPENTER
01CY ATTN G. PRICE
01CY ATTN J. PETERSON
01CY ATTN R. MAKE, JR.
01CY ATTN V. GONZALES
01CY ATTN D. MCDANIEL

TECHNOLOGY INTERNATIONAL CORP
75 WIGGINS AVENUE
BEDFORD, MA 01730
01CY ATTN W. P. BOQUIST

TRW DEFENSE & SPACE SYS GROUP
ONE SPACE PARK
REDONDO BEACH, CA 90278
01CY ATTN R. K. PLEBUCH
01CY ATTN S. ALTSCHULER
01CY ATTN D. DEE

VISIDYNE, INC.
19 THIRD AVENUE
NORTH WEST INDUSTRIAL PARK
BURLINGTON, MA 01803
01CY ATTN CHARLES HUMPHREY
01CY ATTN J. W. CARPENTER

IONOSPHERIC MODELING DISTRIBUTION LIST
UNCLASSIFIED ONLY

PLEASE DISTRIBUTE ONE COPY TO EACH OF THE FOLLOWING PEOPLE:

ADVANCED RESEARCH PROJECTS AGENCY (ARPA)
STRATEGIC TECHNOLOGY OFFICE
ARLINGTON, VIRGINIA

CAPT. DONALD M. LEVINE

NAVAL RESEARCH LABORATORY
WASHINGTON, D.C. 20375

DR. P. MANGE
DR. R. MEIER
DR. E. SZUSZCZEWICZ - CODE 7127
DR. TIMOTHY COFFEY - CODE 6700 (20 COPIES)
DR. S. OSSAKOW - CODE 6780 (100 COPIES)
DR. J. GOODMAN - CODE 7560

SCIENCE APPLICATIONS, INC.
1250 PROSPECT PLAZA
LA JOLLA, CALIFORNIA 92037

DR. D. A. HAMLIN
DR. L. LINSON
DR. D. SACHS

DIRECTOR OF SPACE AND ENVIRONMENTAL LABORATORY
NOAA
BOULDER, COLORADO 80302

DR. A. GLENN JEAN
DR. G. W. ADAMS
DR. D. N. ANDERSON
DR. K. DAVIES
DR. R. F. DONNELLY

A. F. GEOPHYSICS LABORATORY
L. G. HANSOM FIELD
BEDFORD, MASS. 01730

DR. T. ELKINS
DR. W. SWIDER
MRS. R. SAGALYN
DR. J. M. FORBES
DR. T. J. KENESHEA
DR. J. AARONS

OFFICE OF NAVAL RESEARCH
800 NORTH QUINCY STREET
ARLINGTON, VIRGINIA 22217

DR. H. MULLANEY

COMMANDER
NAVAL ELECTRONICS LABORATORY CENTER
SAN DIEGO, CALIFORNIA 92152

DR. M. BLEIWEISS
DR. I. ROTHMULLER
DR. V. HILDEBRAND
MR. R. ROSE

U. S. ARMY ABERDEEN RESEARCH AND DEVELOPMENT CENTER
BALLISTIC RESEARCH LABORATORY
ABERDEEN, MARYLAND

DR. J. HEIMERL

COMMANDER
NAVAL AIR SYSTEMS COMMAND
DEPARTMENT OF THE NAVY
WASHINGTON, D.C. 20360

DR. T. CZUBA

HARVARD UNIVERSITY
HARVARD SQUARE
CAMBRIDGE, MASS. 02138

DR. M. B. MCELROY
DR. R. LINDZEN

PENNSYLVANIA STATE UNIVERSITY
UNIVERSITY PARK, PENNSYLVANIA 16802

DR. J. S. NISBET
DR. P. R. ROHRBAUGH
DR. D. E. BARAN
DR. L. A. CARPENTER
DR. M. LEE
DR. R. DIVANY
DR. P. BENNETT
DR. E. KLEVANS

UNIVERSITY OF CALIFORNIA, LOS ANGELES
405 HILLGARD AVENUE
LOS ANGELES, CALIFORNIA 90024

DR. F. V. CORONITI
DR. C. KENNEL

UNIVERSITY OF CALIFORNIA, BERKELEY
BERKELEY, CALIFORNIA 94720

DR. M. HUDSON

UTAH STATE UNIVERSITY
4TH N. AND 8TH STREETS
LOGAN, UTAH 84322

DR. P. M. BANKS
DR. R. HARRIS
DR. V. PETERSON
DR. R. MEGILL
DR. K. BAKER

CORNELL UNIVERSITY
ITHACA, NEW YORK 14850

DR. W. E. SWARTZ
DR. R. SUDAN
DR. D. FARLEY
DR. M. KELLEY
DR. E. OTT

NASA
GODDARD SPACE FLIGHT CENTER
GREENBELT, MARYLAND 20771

DR. S. CHANDRA
DR. K. MAEDO

PRINCETON UNIVERSITY
PLASMA PHYSICS LABORATORY
PRINCETON, NEW JERSEY 08540

DR. F. PERKINS
DR. E. FRIEMAN

INSTITUTE FOR DEFENSE ANALYSIS
400 ARMY/NAVY DRIVE
ARLINGTON, VIRGINIA 22202

DR. E. BAUER

UNIVERSITY OF PITTSBURGH
PITTSBURGH, PA. 15213

DR. N. ZABUSKY
DR. M. BIONDI